Defense Special Weapons Agency
Alexandria, VA 22310-3398

DSWA-TR-97-4

Instrument Suite to Measure Space and Time Resolved XUV and X-Rays from Z-Pinches

William Guss, Ph.D.
Science Research Lab
15 Ward Street
Somerville, MA 02143

January 1998

Technical Report

CONTRACT No. DNA 001-93-C-0216

DESTRUCTION NOTICE:

Destroy this report when it is no longer needed.
Do not return to sender.

PLEASE NOTIFY THE DEFENSE SPECIAL WEAPONS AGENCY, ATTN: CSTI, 6801TELEGRAPH ROAD, ALEXANDRIA, VA 22310-3398, IF YOUR ADDRESS IS INCORRECT, IF YOU WISH IT DELETED FROM THE DISTRIBUTION LIST, OR IF THE ADDRESSEE IS NO LONGER EMPLOYED BY YOUR ORGANIZATION.

DISTRIBUTION LIST UPDATE

This mailer is provided to enable DSWA to maintain current distribution lists for reports. (We would appreciate your providing the requested information.)

☐ Add the individual listed to your distribution list.

☐ Delete the cited organization/individual.

☐ Change of address.

NOTE:
Please return the mailing label from the document so that any additions, changes, corrections or deletions can be made easily. For distribution cancellation or more information call DSWA/IMAS (703) 325-1036.

NAME: _____

ORGANIZATION: _____

OLD ADDRESS	CURRENT ADDRESS
_____	_____
_____	_____
_____	_____

TELEPHONE NUMBER: (___) _____

DSWA PUBLICATION NUMBER/TITLE	CHANGES/DELETIONS/ADDITIONS, etc.) *(Attach Sheet if more Space is Required)*
_____	_____
_____	_____
_____	_____

DSWA OR OTHER GOVERNMENT CONTRACT NUMBER: _____

CERTIFICATION OF NEED-TO-KNOW BY GOVERNMENT SPONSOR (if other than DSWA):

SPONSORING ORGANIZATION: _____

CONTRACTING OFFICER OR REPRESENTATIVE: _____

SIGNATURE: _____

CUT HERE AND RETURN

DEFENSE SPECIAL WEAPONS AGENCY
ATTN: IMAS
6801 TELEGRAPH ROAD
ALEXANDRIA, VA 22310-3398

DEFENSE SPECIAL WEAPONS AGENCY
ATTN: IMAS
6801 TELEGRAPH ROAD
ALEXANDRIA, VA 22310-3398

REPORT DOCUMENTATION PAGE

Form Approved
OMB No. 0704-0188

1. AGENCY USE ONLY (Leave blank)	2. REPORT DATE	3. REPORT TYPE AND DATES COVERED
	980101	Technical 930928 - 960728

4. TITLE AND SUBTITLE
Instrument Suite to Measure Space and Time Resolved XUV and X-Rays from Z-Pinches

5. FUNDING NUMBERS
C - DNA 001-93-C-0216
PE - 62715H
PR - AB
TA - GI
WU - DH80055

6. AUTHOR(S)
William Guss, Ph.D.

7. PERFORMING ORGANIZATION NAME(S) AND ADDRESS(ES)
Science Research Lab
15 Ward Street
Somerville, MA 02143

8. PERFORMING ORGANIZATION REPORT NUMBER
SRL-1-F-1997

9. SPONSORING/MONITORING AGENCY NAME(S) AND ADDRESS(ES)
Defense Special Weapons Agency
6801 Telegraph Road
Alexandria, VA 22310-3398
EST/Rowley

10. SPONSORING/MONITORING AGENCY REPORT NUMBER
DSWA-TR-97-4

11. SUPPLEMENTARY NOTES
This work was sponsored by the Defense Special Weapons Agency under RDT&E RMC Code B4662D AB GI 80055 5400A 25904D.

12a. DISTRIBUTION/AVAILABILITY STATEMENT
Approved for public release; distribution is unlimited.

12b. DISTRIBUTION CODE

13. ABSTRACT (*Maximum 200 words*)

Science Research Laboratory, Inc. (SRL) had designed, assembled and tested a new suite of X-ray instruments for the PHOENIX radiation simulator. This suite consists of an X-ray pinhole camera, an XUV pinhole camera and an X-ray crystal spectrometer . All three instruments were designed to be located within ≈ 2 - 3 m of a terawatt-class simulator plasma. The instruments provide 0.2 ns continuous time resolution, ≈0.25 mm spatial resolution and a wide dynamic range of ≈ 1000:1. This suite is also capable of measuring the power radiated by the pinch anywhere in a ≈1 μs window, including the very soft (100-900 eV), XUV radiation emitted during the early part of the implosion, and ending with the ≈ 20 ns burst of L- or K-shell X-radiation from different elements, in the 1-15 keV band. The three instruments were assembled, tested, and calibrated using an available 10-20J/pulse X-ray point source of neon K-shell X-rays. To keep costs down, SRL utilized the similarity between the X-ray and XUV pinhole cameras (described in detail later in this report) to build one camera body capable of use both an X-ray and an XUV pinhole camera. In parallel, subcontractors developed and delivered a 224 channel fast array digitizer package with interfaces to the analog output of the SRL suite. Software was also developed to archive data from the digitizer channels and provide preliminary analysis and displays. This suite was installed on PHOENIX and validated.

14. SUBJECT TERMS
XUV Pinhole Camera
X-Ray Pinhole Camera
X-Ray Crystal Spectrometer

15. NUMBER OF PAGES
54

16. PRICE CODE

17. SECURITY CLASSIFICATION OF REPORT	18. SECURITY CLASSIFICATION OF THIS PAGE	19. SECURITY CLASSIFICATION OF ABSTRACT	20. LIMITATION OF ABSTRACT
UNCLASSIFIED	UNCLASSIFIED	UNCLASSIFIED	SAR

NSN 7540-280-5500

Standard Form 298 ((rev. 2-89)
Prescribed by ANSI Sta. 239-18
298-102

CLASSIFIED BY:

N/A since Unclassified.

DECLASSIFY ON:

N/A since Unclassified.

SUMMARY

The main objective of the Phase II program was to develop an integrated suite of instruments based on silicon PIN diode detectors to obtain time and space resolved spectral information about the X-ray and XUV emissions from a Z-pinch plasma. This suite of instruments is radically different from the present MCP based gated instruments that provide information only on the final state of the Z-pinch. It provides information on the early as well as late time behavior of the pinch, allowing new insights into the dynamics of Z-pinches.

CONVERSTION TABLE

Conversion factors for U.S. Customary to metric (SI) units of measurement.

MULTIPLY → / ← TO GET	BY → / ← BY	TO GET → / ← DIVIDE
angstrom	1.000 000 X E -10	meters (m)
atmosphere (normal)	1.013 25 X E +2	kilo pascal (kPa)
bar	1.000 000 X E +2	kilo pascal (kPa)
barn	1.000 000 X E -28	meter^2 (m^2)
British thermal unit (thermochemical)	1.054 350 X E +3	joule (J)
calorie (thermochemical)	4.184 000	joule (J)
cal (thermochemical/cm^2)	4.184 000 X E -2	mega joule/m^2 (MJ/m^2)
curie	3.700 000 X E +1	*giga becquerel (GBq)
degree (angle)	1.745 329 X E -2	radian (rad)
degree Fahrenheit	$t_k = (t^oF + 459.67)/1.8$	degree kelvin (K)
electron volt	1.602 19 X E -19	joule (J)
erg	1.000 000 X E -7	joule (J)
erg/second	1.000 000 X E -7	watt (W)
foot	3.048 000 X E -1	meter (m)
foot-pound-force	1.355 818	joule (J)
gallon (U.S. liquid)	3.785 412 X E -3	meter^3 (m^3)
inch	2.540 000 X E -2	meter (m)
jerk	1.000 000 X E +9	joule (J)
joule/kilogram (J/kg) radiation dose absorbed	1.000 000	Gray (Gy)
kilotons	4.183	terajoules
kip (1000 lbf)	4.448 222 X E +3	newton (N)
kip/inch^2 (ksi)	6.894 757 X E +3	kilo pascal (kPa)
ktap	1.000 000 X E +2	newton-second/m^2 ($N-s/m^2$)
micron	1.000 000 X E -6	meter (m)
mil	2.540 000 X E -5	meter (m)
mile (international)	1.609 344 X E +3	meter (m)
ounce	2.834 952 X E -2	kilogram (kg)
pound-force (lbs avoirdupois)	4.448 222	newton (N)
pound-force inch	1.129 848 X E -1	newton-meter (N·m)
pound-force/inch	1.751 268 X E +2	newton/meter (N/m)
pound-force/foot^2	4.788 026 X E -2	kilo pascal (kPa)
pound-force/inch^2 (psi)	6.894 757	kilo pascal (kPa)
pound-mass (lbm avoirdupois)	4.535 924 X E -1	kilogram (kg)
pound-mass-foot^2 (moment of inertia)	4.214 011 X E -2	kilogram-meter^2 ($kg·m^2$)
pound-mass/foot^3	1.601 846 X E +1	kilogram/meter^3 (kg/m^3)
rad (radiation dose absorbed)	1.000 000 X E -2	**Gray (Gy)
roentgen	2.579 760 X E -4	coulomb/kilogram (C/kg)
shake	1.000 000 X E -8	second (s)
slug	1.459 390 X E +1	kilogram (kg)
torr (mm Hg, 0^o C)	1.333 22 X E -1	kilo pascal (kPa)

*The becquerel (Bq) is the SI unit of radioactivity; 1 Bq = 1 event/s.
**The Gray (GY) is the SI unit of absorbed radiation.

TABLE OF CONTENTS

FIGURES

SECTION 1
INTRODUCTION

Today's above-ground simulator test (AGT) user demands a greater level of detail from the Z-pinch X-ray source, to better benchmark the codes that will help correlate the above-ground tests with underground tests (UGTs). As the new DSWA simulator DECADE becomes operational, there will be a demand for even more detailed characterization of the sources, because of the evolutionary advances in AGT/UGT correlation. If the level of UGTs declines due to test-ban treaties, it will become imperative that the AGT environments be fully characterized, so that the extrapolation from AGT results to UGT predictions and codes is more reliable. Above-ground X-ray simulators produce two types of environments: hard X-rays (20 keV - 1.5 MeV) from bremsstrahlung (brems) diodes and softer X-rays (1 - 4 keV) from Z-pinches. Both types of X-ray sources require more detailed characterization. The diagnostic suite delivered by SRL is restricted to soft X-ray sources from Z-pinches, where the need for detailed measurements is more acute, because of the difficulty of extrapolation from today's drivers to future, higher power drivers. An instrument package that is compact, robust, relatively easy to operate and maintain, flexible and applicable to every simulator will at once enhance the utility of ``user`` tests as well as assist the R&D community to improve existing models for Z-pinch scaling with driver current and power. SRL has developed, tested and installed just such a package on PHOENIX. A spin-off of this technology development would be an affordable yet powerful set of new instruments that can be purchased by other DSWA and DOE facilities, as upgrades to their soft X-ray environments.

Above-ground X-ray simulators produce two types of environments: hard X-rays (20 keV-1.5 MeV) from brems diodes and softer X-rays (1 - 4 keV) from Z-pinches. The soft X-rays from Z-pinches are used to test front surface phenomena. Existing DSWA simulators such as Double-EAGLE (DE), BlackJack-5 (BJ-5) and PHOENIX can produce ~50 kJ/pulse of neon K-shell X-rays (0.9 - 1.4 keV), ~ 40 kJ and aluminum K-shell X-rays (1.6 - 2 keV) and ~15 kJ of argon K-shell X-rays (3.2 - 4 keV). These outputs are

produced by imploding a cylindrical array of fine wires or a supersonic shell of gas from ~ 1.5 - 3 cm initial diameter, to form a tight pinch ~ 2 - 3 mm in diameter and 4 cm long, on the axis of a coaxial diode. The implosions are driven by a ~ 3.5 MA current that has a 90 ns rise-time, from a Marx bank driven pulse-line. Figure 1-1 shows a schematic drawing of the concept. Figure 1-1 (a) shows the end view of the initial wire array load configuration. Figure 1-1 (b) shows the side view and the final pinch state. Figure 1-2 shows a typical current trace and a superimposed trace of X-ray emission from the pinch. The X-rays in this case are observed to occur during a ~ 40 ns time interval, near the peak of the current pulse. About 400 kJ of total energy is coupled from the pulse-line to the Z-pinch diode. Of this, about 60 kJ is in the form of kinetic energy of the radially accelerated plasma, the rest being magnetic energy around the pinch and in the vacuum transmission line from the insulator to the diode region. When the radially moving plasma assembles on the axis, some of the kinetic energy is converted into K-shell X-rays, provided that the temperature of the assembled plasma is high enough to ionize the shell mass into the K-shell. In addition, a fraction of the magnetic energy is also tapped by the pinch *via* resistive heating, to augment the K-shell emission. Whereas the neon plasma (~ 1 keV X-rays) apparently taps about 12% of the total electrical energy injected into the vacuum, this fraction drops to 10\% for the aluminum plasma (~ 1.6 keV X-rays), and even lower to ~4% for the argon plasma (~ 3.2 keV X-rays). A higher current DOE driver, SATURN, has been used to produce X-ray bursts from the same elements as the DSWA simulators. The absolute outputs are higher from SATURN; 100 kJ of neon K-shell X-rays, 70 kJ of aluminum K-shell X-rays, and 40 kJ of argon K-shell X-rays. However, when these outputs are expressed as fractions of the electrical energy (750 kJ) injected into the vacuum, they are roughly similar (13% Ne, 9% Al and 5% Ar) to the lower current DSWA simulators. The next DSWA simulator to be built will be DECADE, which will inject ~ 4 MJ of total energy into Z-pinch diodes, at currents of ~ 20-25 MA. If the fractions measured at 3.5 MA on DE and BJ-5 as well as at 9 MA on SATURN remain the same for DECADE, then one can project K-shell outputs of ~ 600 kJ of aluminum and ~ 360 kJ of argon from DECADE, with loads designed to give the proper end-state densities and temperatures.

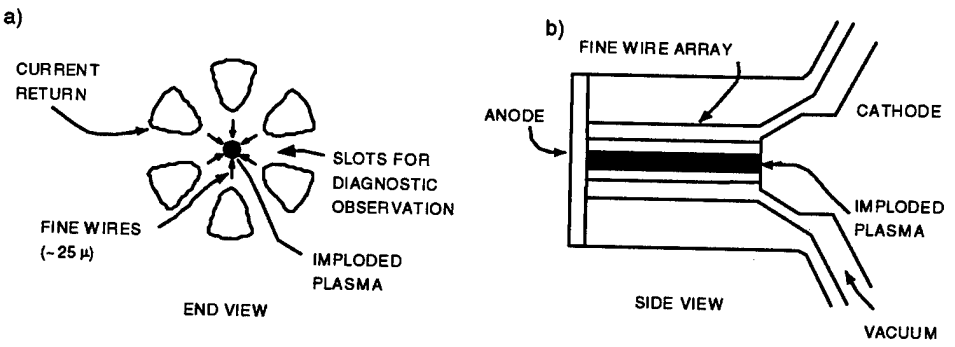

Figure 1-1. Schematic drawing showing the formation of a Z-pinch. (a) End View of the intial wire array load configuration. (b) Side view and final pinch state.

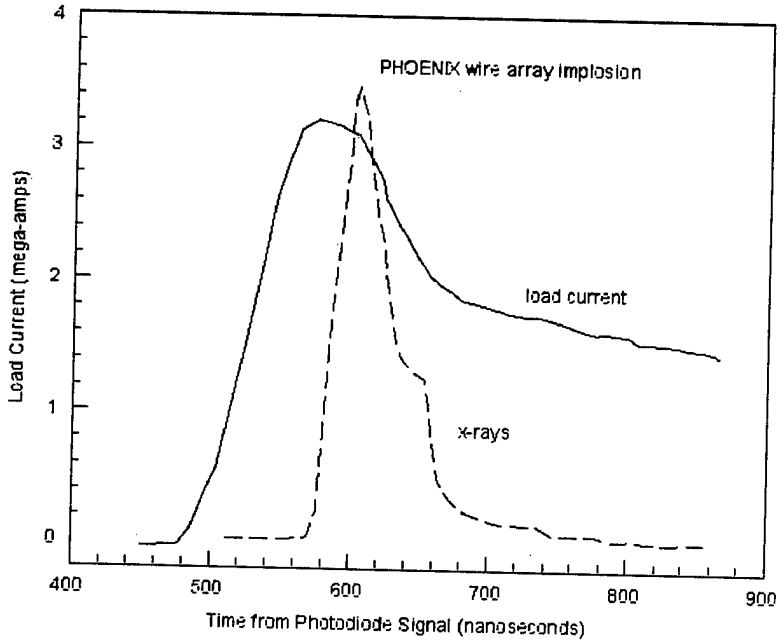

Figure 1-2. Typical load current and X-ray output traces from PHOENIX.

While these outputs are attractive and meet the present requirements for soft X-ray environments on DECADE, they are worthy of further improvement. The problem is that the physics of the implosions is not understood well enough to apply reliable scaling laws from one machine to the next. One reason for this is that the details of the implosion are not usually studied from start to finish. To motivate the design methodology for Z-pinch (PRS) loads, Figure 1-3 shows how one approaches the design task. Exactly as is the case

for the brems designs, the radiation requirements narrow the design parameters for the PRS loads. The desired spectrum determines the atomic number of the PRS load elements. For K-shell radiators, the atomic number demands a certain range of electron temperature T_e and electron density η_e, to ionize all the ions into the K-shell, producing a mean charge **Z**. For example, a ~ 200 eV plasma is adequate to ionize a neon pinch into the K-shell, but ~ 600 eV is required for an aluminum, K-shell plasma, increasing to ~1 keV for argon and ~ 2.5 keV for copper. These temperature in turn demand a minimum specific energy (final radial velocity) per ion as the pinch assembles on axis. The ion density ρ_i and size r of the pinch plasma are determined by the requirement that the K-shell X-rays be emitted within a prescribed time interval, ≤ 30 ns. A given yield from a given temperature plasma corresponds to some net radiative rate for K-shell emission, which determines the required ion density ρ_i and size r of the pinch. The radiation specifications (spectrum, output and pulse width), therefore, completely specify the desired end-state of the pinch plasma, ρ_i, T_e, r and **Z**.

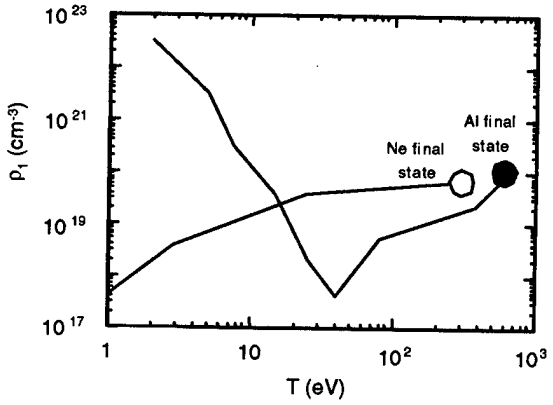

Figure 1-3. Design methodology for Z-pinch loads.

The designer's task is to choose the right initial configuration of the load that will reach the desired end-state, when driven by the particular electrical driver.

All the complicated physics of PRS loads is in the path followed by the imploding loads from the initial to final states. Figure 1-3 shows two representative trajectories in the ρ_i-T

phase space that might be followed by imploding plasma loads of neon or aluminum. The aluminum load starts at solid density and room temperature, expands early in the pulse to a ~ 1-10 eV plasma at much lower density, then implodes and increases in density towards the end of the current pulse. The neon gas puff load starts as a weakly ionized plasma and increases in density and temperature as it approaches the axis. Hydromagnetic instabilities such as Rayleigh-Taylor modes and diffusion of the driving magnetic field through the shell early in time can spoil the quality of the implosion, resulting in poor output.

The scale the PRS load geometry from one machine to the next, one needs to know how these instabilities scale with current, energy, initial radius, aspect ratio and initial conditions such as the degree of pre-ionization of the shell. Although elaborate theoretical models have been developed over the past decade[1,2], simple but useful dimensional similitude relations have not been extracted from these models, that would enable the load designer to set the initial radius, mass, aspect ratio and current rise-time in such a manner as to predict the desired end-state values of , ρ_i, T_e, r and **Z** for a particular K-shell radiator, taking into account the growth of instabilities and turbulence in the medium. Part of the problem is the vast excursions in density-temperature space that are followed by the imploding loads. Another part of the problem is that radiation plays an important role in determining the final state. The medium is usually optically thick to the radiation. Gradients in density and temperature make the radiative transfer problem difficult to treat within a simple theoretical framework. Theoretical models will be greatly simplified if more detailed measurements are made of the entire trajectory in ρ_l -T space followed by the implosion.

Available instruments tend to focus on the end-state of the implosion, when the K-shell X-ray emission occurs. But the efficiency with which the pinch converts the available reservoir of energy into K-shell X-rays is determined by the detailed history of the density and temperature followed by the pinch during the radial motion, as well as by the end-state. Better measurements are needed of the motion of the shell from its initial state to the final state, so as to develop more accurate models of the essential physics. A typical gas shell such as an argon shell goes from ~ 1 eV temperature early in time to ~ 1 keV temperature in the final assembly. The plasma thus emits radiation over a broad spectrum,

from UV (~ 10 - 100 eV) and XUV (~ 100 - 500 eV) emissions early in the implosion, to soft X-rays (~ 3 - 4 keV) later in time. All these emissions occur within a ~ 50 - 100 ns time interval, over a ~ 1 - 2 cm radial extent.

Instruments are therefore required that can capture such emissions with <3 ns time resolution and ~ 0.5 mm spatial resolution, as well as with adequate spectral resolution. As mentioned above, the DSWA and DOE simulators, at present, rely on gated MCP detectors[3] to provide temporal resolution of X-ray pinhole camera images of the assembled pinch and of X-ray spectra from crystal spectrometers. The problems with MCP/film based detectors are that they are delicate instruments, requiring highly skilled operators and are difficult to interpret quantitatively because of the highly non-linear response of the MCP detectors and film. Further, the dynamic range of these detectors is limited, when used in conjunction with film, to ≤ 30:1. The silicon PIN diodes delivered by SRL require only ≤ 50 V bias voltages, whereas the MCP require ~ 1 kV gate pulses and several kilovolts bias voltage for the accompanying phosphors. Since the PIN diode bias is a relatively low dc voltage, the PIN diodes can even be operated at atmospheric pressure, unlike MCP based instruments, which demand clean and fairly high vacuums.

The new instruments delivered by SRL overcome the limitations of MCP based detectors, as well as shed light on Z-pinch physics, to enable more efficient load designs for tomorrow's PRS simulators such as DECADE and JUPITER. Whereas PHOENIX, DE and BJ-5 are pulse-line driven, DECADE PRS loads will be driven by an inductive store (IES) current source. The physics of implosions with such IES sources will be very different from the conventional pulse-line driven sources, another reason to have at hand an instrument suite that can capture the details of the implosion from start to finish. How are IES driven implosions different from pulse-line driven implosions?

In pulse-lines such as PHOENIX, BJ-5 and SATURN, the current pulse shape is nearly independent of the load dynamics during most of the radial run-in. Only near the very end of the acceleration, when the pinch assembles on axis, does the impedance of the load react on the circuit. Because the driving current always decays after a fixed interval in a pulse-line, the designer must accept a fixed implosion time in order to assemble the pinch near maximum current. Changing the initial radius of the shell then *forces* the mass to be

changed, to keep the implosion time fixed, for a fixed current. This in turn changes the final velocity (specific energy) of the ions. The different masses and velocities result in different density-temperature products for a given current. There is an optimum radius and mass that together maximize the K-shell output, while giving just the minimum required specific energy for a given radiator to be fully ionized into the K-shell, also allowing for M and L-shell losses along the way. Smaller radii with higher masses produce denser plasmas that are too cold and radiate less than the optimum, while larger radii with smaller masses produce hotter but less dense plasmas which in turn also radiate less than the optimum. Such an optimum was determined for nickel and aluminum wire arrays experimentally[4,5] on E=DE and analyzed theoretically[6]. The situation is very different when a plasma opening switch (POS) from an IES driver such as DECADE, is coupled to a PRS load.

The rise-time of the current from a POS to an imploding plasma load will change as the load mass and initial radius are changed, because the rate of rise of current into the load (or current shunted out of the POS) can alter the rate of opening of the switch. This strong coupling between the load and the switch *throughout* the radial motion makes it possible to design PRS loads that are not constrained in the same way as for pulse-lines. For example, one can increase *both* the mass and the radius of the shell, while still keeping the final velocity and current constant, by letting the implosion time (and current rise-time) increase. This is an important design feature for IES drivers, for it is advantageous to maximize the pinch mass and thus the radiated output. The only practical limit to increasing the implosion times for larger initial radii is the stability of the implosion. For advanced PRS simulators like JUPITER, a critical design feature is to establish whether long (150 - 300 ns) implosions are stable and efficient. The payoff in reduced cost, added reliability and simplicity will be significant.

To explore these innovations in load designs for IES drivers requires detailed measurements of the implosions, across the entire spectrum from UV to XUV to soft X-rays. Again, this requirement motivated the SRL development of the diagnostic suite. The next section details the objectives of this project.

SECTION 2
TECHNICAL APPROACH

The design of this suite marks a departure from existing X-ray instruments for Z-pinches and other pulsed, bright, soft X-ray sources. The SRL suite offers spatial resolution, *continuous* (rather than gated) time resolution, and covers emissions over the entire course of the PHOENIX implosion, from XUV (100 - 900 eV) to soft X-rays (1 - 15 keV). The basic detector element for all these instruments is a fast silicon PIN diode arranged in 2-dimensional arrays of up to 100 (10 X 10 array). These diode arrays offer 1000:1 dynamic range, $\leq$ 1 ns time resolution with a continuous read-out, and provide a *constant* response over the entire range of measured emissions, from 100 eV to 15 keV and beyond. The innovative approach described here for the design of new X-ray instruments was complemented by innovations in digitizer architecture, to capture the large number (up to 224) of channels of analog data from the PIN diode array, in a compact, dedicated digitizer module that can be located close to the instrument suite and allows a fast I/O interface for transfer of the digital data to other post-processor modules such as the local computer network at PHOENIX or a dedicated micro-computer.

This suite is designed to replace existing X-ray instruments that rely on gated micro-channel plate (MCP) detectors. Both DOE (SATURN) and DSWA Double-EAGLE) simulators presently capture soft X-ray emissions from Z-pinches using MCPs that are gated with $\approx$1-5 ns gate pulses. By spacing the gate pulses apart in time, time-gated data are obtained over the duration of the Z-pinch emission. These MCPs convert incident X-rays into electron bursts. Time resolution is provided by ~ 1 kV, 1-5 ns gate pulses applied to the MCP face by Krytron pulsers. The electrons from these MCPs are proximity focused onto a fiber-optic bundle whose face is covered with a P-11 phosphor. The visible light output from the fiber bundle is then captured on 35 mm film. Because the gain of the MCPs depends very strongly on the applied voltage $\approx V^{10}$, these instruments have a very limited dynamic range. Such MCP based instruments have helped to improve our understanding of Z-pinch physics, but they have been primarily used to study the *final* state of the implosion, when the pinch plasma emits soft X-rays in a ~ 30 ns burst.

Typically, only a few ~ 5 ns time frames of emission from a Z-pinch are captured, and even these are often saturated, making quantitative analysis difficult. The typical imploding plasma Z-pinch emits radiation from ~ 1 eV to ~few keV, as it passes from an initial temperature of ~ 1 eV to a final temperature ~ 1 keV. This spectrum of emission occurs over the entire duration of the implosion, ~ 50 - 120 ns. The efficiency with which the final pinch plasma converts the available reservoir of electrical energy (both kinetic and magnetic) into soft X-rays for effects testing, is strongly dependent upon the initial conditions of the load, and the manner in which the imploding plasma assembles on the axis. Although many detailed theoretical treatments of the implosion exist,[2,7] there is a lack of useful scaling laws or parameters with which the load designer may optimize a *given* load on a *given* simulator. While the MCP based instruments, including X-ray crystal spectrometers, XUV grazing incidence grating spectrometers and X-ray pinhole cameras have enhanced the available data base, the detector elements are fragile and have required highly skilled personnel for their operation and maintenance. As a result, they are not used in routine support of ``user" tests on the DSWA simulators. These simulators still rely on time integrated spectra and pinhole images of the pinch, as standard complements to filtered X-ray diode arrays, bolometers and calorimeters, which together measure the X-ray output of the pinch in different spectral bands.

The new type of X-ray suite developed by SRL allows the designer a first look at the early time dynamics of the implosion, *via* the XUV pinhole camera. Key questions, such as, whether and how quickly the wires in a wire-array are ionized and expand to fill out the azimuth, what is the thickness of the current carrying sheath in a pre-ionized gas puff, when does the load region of the magnetically insulated transmission line (MITL) suffer radiative hole closure, and other issues will be better understood with such XUV measurements. The X-ray pinhole camera will provide $\geq$ 250 μm spatial resolution of the final pinch, along with $\approx$ 2 ns temporal resolution ($125 MHz analog bandwidth from a 500 MS/s (MS/s} = MSamples/s) digitizer board. The X-ray crystal spectrometer was designed to be flexible and yet simple to operate, with interchangeable crystals to cover the energy range from $\approx$1-15 keV.

SRL began development of this extended suite *via* a DSWA Phase I SBIR contract, #DNA001-92-C-0102, during the period 9-22-92 to 3-21-93. Under this contract, a crystal spectrometer was built, with a linear array of eight PIN diodes designed to capture eight spectral bands of emission from the K-shell of neon pinches. This time resolved spectrometer was validated on a 10-20 J neon X-ray point source at SRL.

As part of the Phase II program, the linear detector of the crystal spectrometer was upgraded to a 2-dimensional PIN diode array in order to add spatial resolution to the time resolved instrument, as well as to build the X-ray and XUV pinhole cameras, also with 2-D detector arrays. This suite of instruments was tested at SRL and subsequently field tested and delivered to the PHOENIX simulator at the Naval Surface Warfare Center, Silver Spring, Maryland. The detector package uses a 10 X 10 array of PIN diodes for the pinhole cameras and a 3 X 8 array for the crystal spectrometer to give up to a total of 224 pixels of information. An innovative data acquisition approach was delivered that allows the use of seven digitizer boards in a standard VXI bus, each with 32 channels of 500 MS/s digitizers, to capture all 224 pixels of data from each shot. The integrated instrument suite, including data acquisition hardware and software, was developed as a flexible package that can be used as a stand alone sub-assembly, or easily integrated into the available data acquisition system at PHOENIX.

The three instruments can be mounted either singly or in parallel at the end of a single beam-line, leaving maximum access to the pinch for ``user`` test objects, debris shields and other instruments. At a distance of about 2 m from the PHOENIX Z-pinch, this suite occupied a space of about 30 cm x 30 cm x 30 cm. The same concept can be designed and deployed on other DSWA and DOE simulators, to complement existing instruments.

An important feature of the SRL suite of instruments is that it is not specific to PHOENIX. The same suite could just as easily be installed on any other existing simulator (BlackJack-5, Double-EAGLE, SATURN or PHOENIX). This suite can also be used on a PRS test-bed such as ACE-IV, in support of scaling research for JUPITER. Indeed, the fact that the delivered suite was tested initially on a 20 J source at SRL and subsequently used on a 40 kJ source such as PHOENIX is proof of the flexibility and wide dynamic

range of the instruments. The suite should be viewed as a versatile package that is universally applicable to any present or future simulator.

Figure 2-1 shows a block diagram depicting the interface with PHOENIX, the instrument suite, and the data acquisition and analysis package. The *only* part of this entire system that was provided GFE was the PHOENIX vacuum chamber and PHOENIX test time. The interface with PHOENIX, the instrument suite, the digitizers, the GPIB interface between the digitizers and the micro-computer, the micro-computer for data acquisition and analysis, the data acquisition and analysis software and printer for hard copy data procured in the Phase II program. This section presents a detailed technical description of the effort. In Section 2.1 the physics of silicon PIN diodes, the basic detector element used in the three instruments, is reviewed. Section 2.2 presents the principles of operation of the X-ray and XUV time resolved imaging cameras. The crystal spectrometer design is presented in Section 2.3. In Section 2.4 the data acquisition system including the array digitizers, the data acquisition software and the image analysis software is discussed.

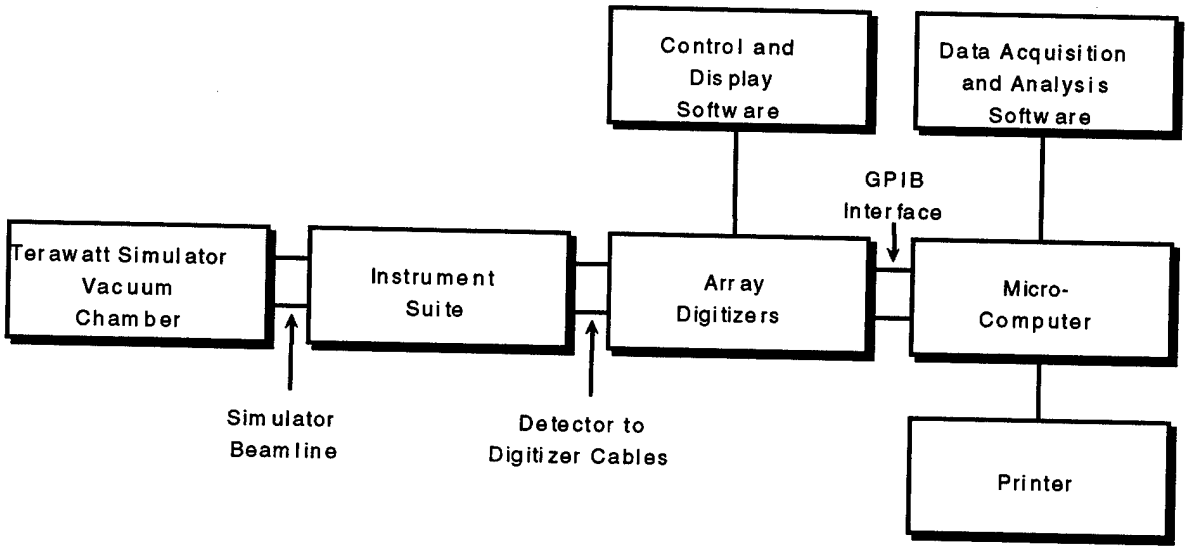

Figure 2-1. Schematic diagram of a X-ray diagnostic suite and digitizer system.

2.1 SILICON PIN DIODE X-RAY DETECTORS.

Silicon PIN diode detectors are made from ultra-high purity silicon (nearly intrinsic) using a double diffusion technique where a heavily doped P-layer is diffused into the rear face of

the silicon and a lightly doped N-layer is diffused into the entrance face obtaining a so called PIN diode structure. The diodes are operated under ~200 VDC reverse bias. Photons interact in the I-layer by means of the photoelectric and Compton effects to produce electron-hole pairs. Motion of these charges in the field results in a current in the external load, usually a 50 ohm coaxial line terminated in 50 ohms at an oscilloscope or digitizer. The output voltage developed at the load reproduces the temporal properties of the photon source, within the bandwidth of the electronics, while the integral of the voltage is a measure of the absorbed energy.

The sensitivity of a silicon PIN diode detector depends only on the probability that a photon incident on the detector reaches the intrinsic layer and the probability that it interacts with the silicon. Calculations have been made that determine the probability of the interaction with the silicon[8]. This function is a very weakly varying function of the incident photon energy for photon energies less than 10 keV. Thus the detector sensitivity is almost a constant and is given by:

$$S(E) = 0.276 F(E) \quad \text{Coulombs/J} \tag{2.1}$$

where F(E) is the transmission of the dead layer of silicon on the entrance face. Most PIN diodes have this dead layer of silicon at the entrance face, which acts as a pre-filter to the photons incident on the diode. Since the transmission of silicon in the XUV is a strong function of photon energy these diodes are not usable in that wavelength range. Recent advances in diode technology have enabled the elimination of this dead layer. Work carried out at International Radiation Detectors under a DOE SBIR has developed PIN diodes with no dead layer. These have a sensitivity of 0.276 Coulombs/J from the uv through 10 keV, i.e. they provide a *constant* detector response over the *entire* wavelength range of emissions of a Z-pinch, from start to finish. This is a unique feature of PIN diodes, shared only with photo-conducting detectors (PCDs).

The power emitted by the PRS in radiation of wavelength λ can be inferred from the diode signal in any of the instruments by,

$$P(\lambda,t)=\frac{1}{T(\lambda)\eta(\lambda)}\frac{50\Omega}{V_{PIN}(t)}\frac{4\pi r^2}{A_{PIN}}\frac{1}{R_{eff}} \tag{2.2}$$

where $\eta(\lambda) \approx 0.276$ A/W is the PIN diode quantum efficiency (Fig. 2.1), $V_{PIN}(t)$ is the PIN diode voltage at time t, $50\Omega/V_{PIN}$ is the PIN diode current, r is the source to diode distance, A_{PIN} is the diode area, $T(\lambda)$ is the filter transmission. The last factor, R_{eff} is the effective reflection coefficient and has the following values for the different instruments:

$$\begin{aligned} R_{eff} &= \varepsilon_g(\lambda) && \text{Spectrometer} \\ &\approx 0.8 && \text{XUV Camera} \\ &= 1 && \text{X-Ray Camera} \end{aligned} \tag{2.3}$$

where $\varepsilon(\lambda)$ is the grating efficiency for Bragg reflection. The reflection coefficient is unity in the X-ray camera because there is no reflecting surface after the filter, and the reflection coefficient is near unity for the XUV camera because of the characteristics of the nickel-coated grazing-incidence mirror. The PRS yield is then,

$$Y(\lambda,t)=\int_0^t P(\lambda,\tau)d\tau \tag{2.4}$$

2.2 X-RAY AND XUV TIME RESOLVED IMAGING CAMERAS.

X-ray images of Z-pinch plasmas are typically obtained by placing a pinhole some distance *u* from the pinch and placing X-ray sensitive film at a distance *v* from the pinhole. The pinhole is covered by a filter such as thin foils of aluminum or beryllium, to block emissions in the visible, UV and deep-UV parts of the spectrum. An image of magnification *v/u* of the X-ray emissions from the plasma is captured on the film. This provides a time-integrated record of the emissions from the plasma. In order to time resolve these images, practically the entire DSWA/DOE simulator/ICF community has used gated MCPs on phosphor screens and multiple pinholes to obtain multiple images of the pinch, each being integrated over a small but finite duration of time. The images generated on the phosphor screen are captured on film and later digitized. There are some drawbacks to this approach of obtaining time resolved images.

Firstly, the dynamic range of the MCPs is small. As a result, it is very difficult to perform quantitative analyses of the captured images, since they are typically either saturated or totally absent. Secondly, the images are captured first on film and subsequently digitized. This introduces uncertainty in any quantitative estimate of the intensity of the image captured due to the highly non-linear nature of the film development process. Additionally, as pointed out earlier, MCPs are expensive and rather delicate instruments.

In each of the pinhole cameras, SRL used an array of silicon PIN diodes instead of the X-ray sensitive film or the MCP based framing cameras. In other experiments at SRL, we have determined that PIN diodes have a large dynamic range, in excess of 1000:1 and offer a continuous rather than gated measure of the incident photon flux. Until recently, however, the problem with using PIN diodes in an imaging application was the lack of availability of diode arrays. Today, PIN diode arrays made from a single silicon crystal, with rectangular pixels, and no dead zones between pixels are available. SRL used a 10 X 10 array of PIN diodes, each 1 mm X 1 mm. Figure 2-2 shows the concept and Figure 2-3 show a photograph of the X-ray camera. The outputs of the 100 diodes are separately digitized using the 224-channel fast digitizer package discussed below, and stored on a computer. This gives a calibrated measure of the X-ray emission from the pinch as a function of space and time, within seconds of the shot.

The pixel resolution of the diode array developed by SRL is 1 mm X 1 mm. The entire image plane is 10 mm X 10 mm. With the pinhole and diode array plane configured for 4:1 magnification a 2.5 mm X 2.5 mm region of the pinch will be imaged at a 250 μ m pixel resolution.

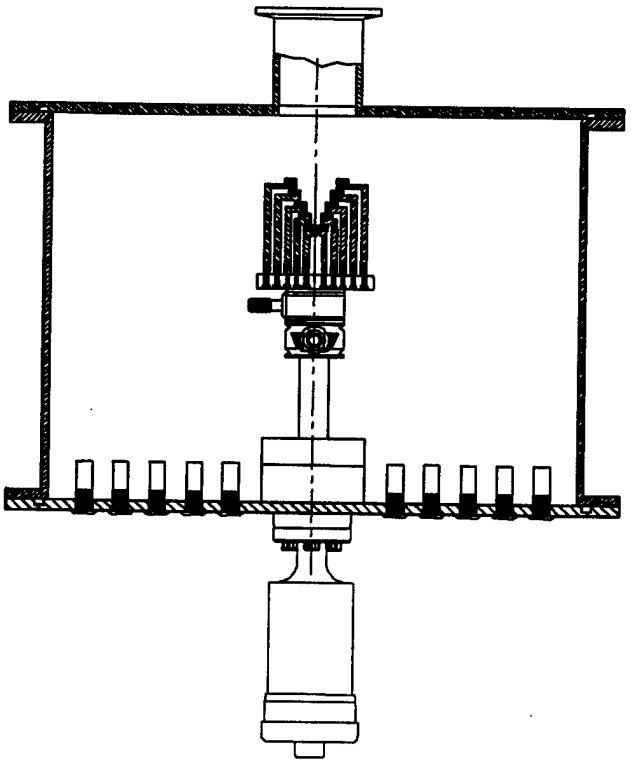

Figure 2-2. Schematic diagram of the X-ray pinhole camera design.

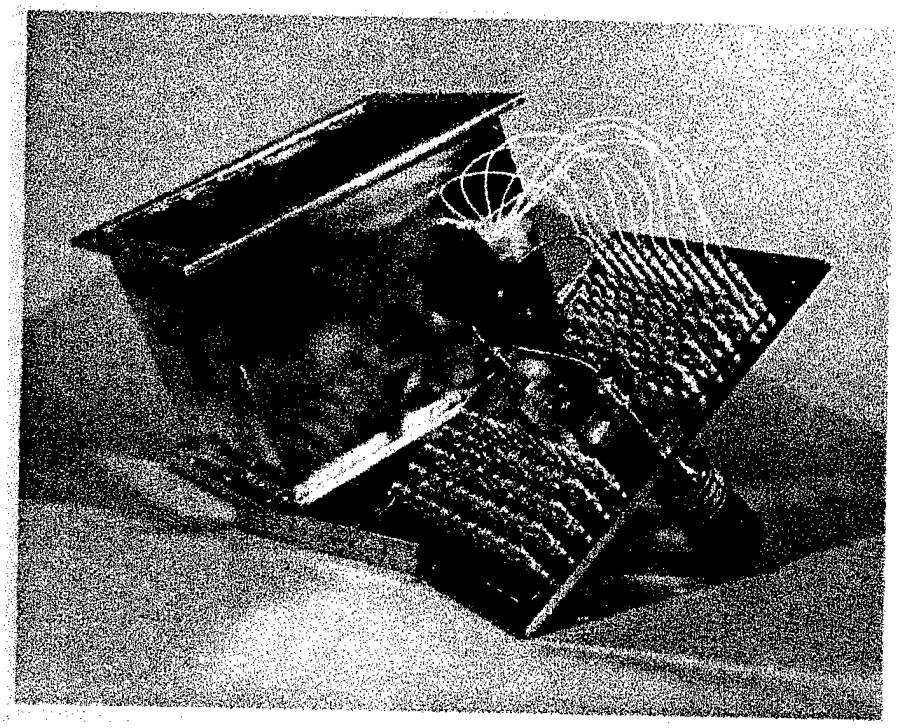

Figure 2-3. Photograph of the X-ray pinhole camera with two PIN diode chips installed.

Position of the diode array is externally adjustable, the lower handle in Figure 2-2, to facilitate fine positioning of the array during experimental operation. In addition, SRL delivered three sets of diode holders which provided three different spacings of the diode strips for various axial spacings of the diodes. The closest axial spacing equaled the radial spacing of the diodes on each chip (1 mm), the intermediate spacing provided an axial separation of 2 mm, and the largest axial spacing provided and axial separation of 4 mm between each chip. The total axial extent for the closest spacing was 1 cm, and the total axial extent of the coarsest spacing was 4 cm.

Table 2-1 shows the configurations of the pinhole camera and filters that might be used on DECADE with loads of aluminum, argon, copper, and krypton and the expected signal strengths. Also shown is the configuration used with the SRL neon source to test the pinhole camera. The pinhole diameters and filters are adjusted in order to produce a diode signal of ~ 1 V, since the array digitizers (described in Section 2.4) have a 1 V peak-peak input range. Signals larger than 1 V can be easily attenuated, either by means of passive attenuators at the digitizer input or by increasing the thickness of the X-ray filters located near the pinholes. The table shows the case when the PIN diode array is located 3 m from the Z-pinch. If space constraints require that the diode array be located 2 m from the source, the signal strengths would be a factor ~ 2 larger than those shown in Table 2-1. These larger signals can be attenuated easily in the manner discussed above. In the event that the diode array has to be located further away from the source, say at 4 m, the signal strengths would still be large enough to be easily read above the digitizer noise, due to the large dynamic range of the digitizers and PIN diodes.

Table 2-1. Configurations of Pinhole Diameters and Filters for the X-Ray Camera.

	Terawatt Simulator				SRL
	Al	AR	Cu	Kr	Ne
K-Shell Energy (keV)	1.5-2.5	3.2-4.5	8.4-10	13.2-15.0	0.92-2.0
K-Shell Output (keV)	600	360	1060.015		
Magnification	3-4	3-4	3-4	3-4	4
Pinhole (μm)	4	4	4	4	0.75
Filter	12μm Ti	75μm Ti	150μm Ti	200μm Ti	25μm Ti
Signal (V)	1.1-0.65	0.7-0.35	0.5-0.25	0.7-0.4	0.7-0.5

The XUV imaging camera (shown in Figure 2-4) uses the same principle as the X-ray imaging camera. In fact, the X-ray camera chamber is identical with the XUV chamber. The capability of variable axial spacing of the diode array is also available in the XUV camera. Unlike the X-ray camera, the XUV camera utilizes two filters to create a bandpass transmission characteristic for the vacuum ultraviolet portion of the spectrum. In order to separate the XUV emissions from the X-ray emissions a grazing incidence mirror was used. Figure 2-5 shows the specular reflectivity, at near grazing incidence, of nickel. At a given energy, for instance 800 eV, radiation incident at angles less than the critical angle $\approx$ 40 mR, is reflected. At angles larger than the critical angle incident radiation is scattered to all angles and does not reach the camera diode array. It is clear from the figure that at an angle of $\geq$40 mR, from grazing incidence, radiation harder than 800 eV-1 keV is effectively cut off, *i.e.* the mirror is effectively a band-pass filter for XUV radiation. The radiation transmitted by this band-pass filter is collected by the PIN diode array.

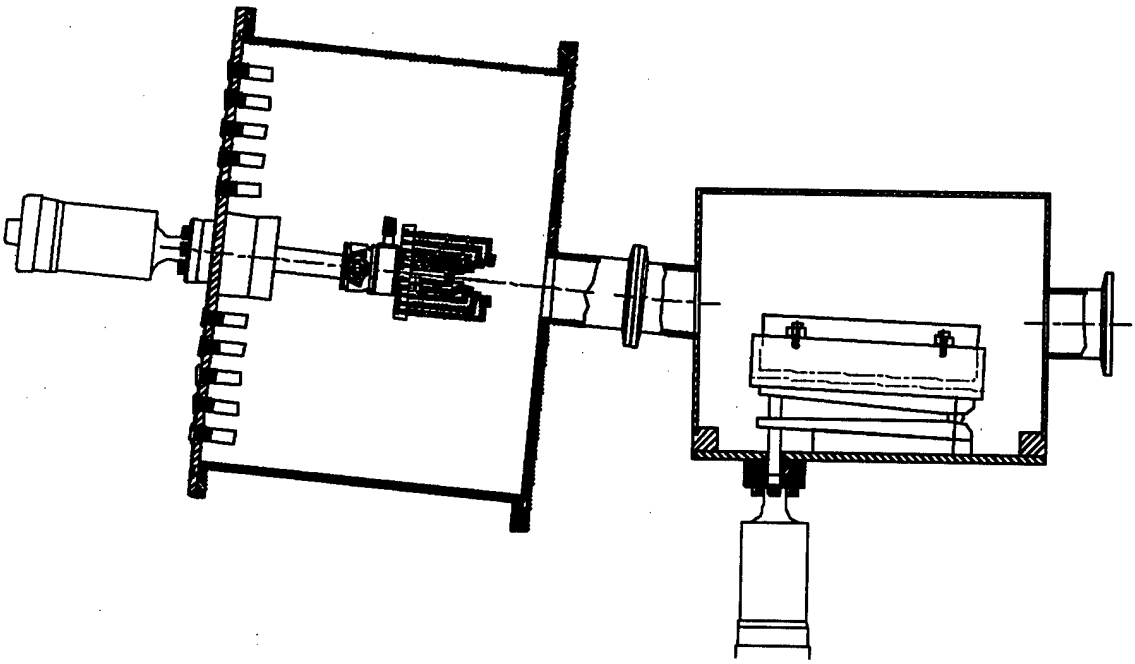

Figure 2-4. Schematic diagram of the XUV camera design.

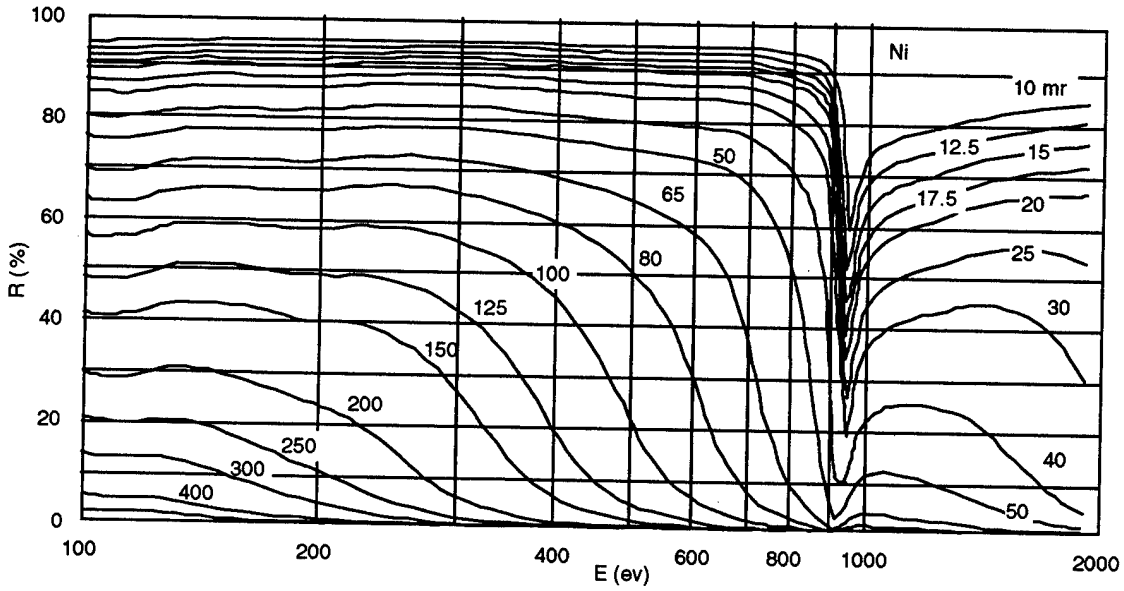

Figure 2-5. Calculated reflectance for incident angles above a nickel mirror surface.

The PIN diode array incorporated in the XUV camera has an important difference from the array proposed for the X-ray camera. Conventional PIN diodes, of the kind proposed

for the X-ray camera, have a dead layer of silicon ~ 0.5 μ m thick. While this does not seriously attenuate X-rays of energy 800 eV and greater, it strongly attenuates photons in the range 100 - 500 eV. Recently, under a DOE SBIR, International Radiation Detectors has developed PIN diodes[10] that do not have this dead layer and thus have a flat response all the way to the visible part of the spectrum. SRL used a 10 X 10 array of these PIN diodes to obtain the time resolved XUV images.

Using a reflectivity of 10%, a magnification ratio of 1:1 and no filter, the signal strengths expected from the diodes in the array can be calculated as a function of the XUV radiation emitted by the pinch. Table 2-2 shows these expected signal strengths. To calculate these signal strengths it was assumed that a 2000 Å aluminum layer would be deposited on the PIN diode array to block visible light. This filter reduces the XUV radiation impinging on the diode array by about a factor of 3. As in the case of the X-ray pinhole camera, the larger signals can easily be attenuated to fit the digitizer input range of 1 V peak-peak.

Table 2-2. Configurations of Pinhole Diameters for the XUV Camera.

	Terawatt Simulator				SRL
	Al	Ar	Cu	Kr	Ne
XUV Output (kJ	400	100	50	10	0.015
Magnification	3-4	3-4	3-4	3-4	4
Pinhole (μm)	125	125	125	125	125
PIN Distance (m)	3	3	3	3	1
Signal (V)	3-9	1.5-5	1.25-3.75	0.3-1	0.05-1

The fundamental difference between the XUV and X-ray camera diodes is the presence of this filter material to be used on the XUV camera diodes which would block the visible emissions from the plasma. Unfortunately, masking and etching problems in the chip fabrication process prevented 100 diodes from being produced. Instead thin free-standing filter material (paraline) mounted at the pinhole was used instead.

2.3 DESIGN OF THE SPACE AND TIME RESOLVED X-RAY CRYSTAL SPECTROMETER.

This section outlines the design of a curved crystal spectrometer, primarily to study neon implosions, but which can be easily modified to study emissions from other implosions in the 0.003 - 17 Å wavelength region. A time resolved version of the spectrometer has already been developed and validated under the Phase I effort. The details of the design were presented in the Phase I Final Report[11] and are not reproduced here. Only the conceptual design, the details of the dispersion expected from the instrument and photographs showing the completed spectrometer are presented for completeness. Finally, the design modifications to add spatial resolution to the spectrometer are discussed.

2.3.1. Design.

Figure 2-6 shows the conceptual design of the X-ray crystal spectrometer. This instrument uses a rigidly mounted crystal and detector plate that can either be a DEF film holder or an array of PIN diodes (discussed later in the text), arranged so as to capture wavelengths of interest in the spectrum, in a box with dimensions of 20 cm X 15 cm X 7.5 cm deep. While providing complete versatility, yet keeping the design simple and robust, only two adjustments are provided for the crystal mount. One is to allow for shims of various thicknesses to be placed under the crystal mount. As shown in Section 2.3.2, varying the point of incidence on the crystal face of the central ray from the source, changes the central wavelength on the detector plate. This allows X-ray spectra of different elements to be centered using different shims. The second adjustment is to correct for any possible beam-line misalignment. The crystal mount is provided with the ability to pivot about an axis along the direction of the beam-line.

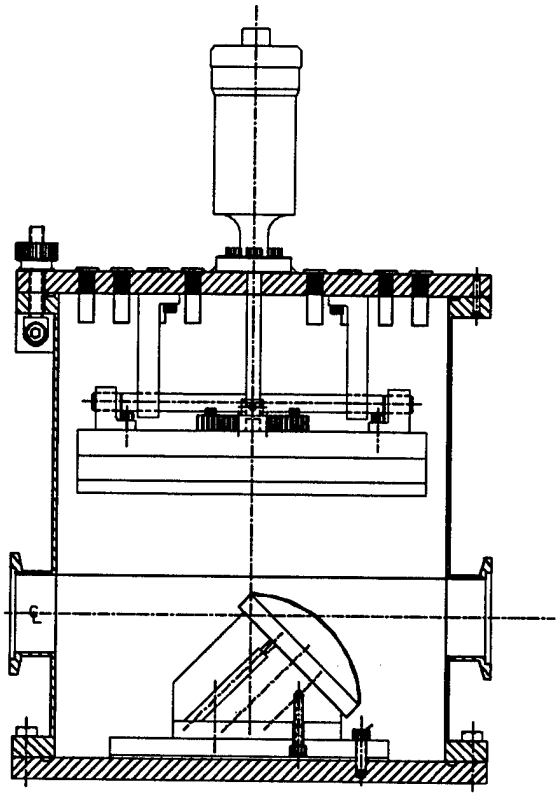

Figure 2-6. Schematic diagram of the bent-crystal spectrometer design.

Using KAP, MICA and LiF crystals, and shims of 2.8 and 8.5 mm thicknesses, this instrument can cover K-shell spectra from ~ 1 keV (Ne) all the way up to ~ 9 keV (copper). Using other shims, it is possible to design for the central wavelength to be appropriate for krypton (~ 0.9 Å) if needed, with a LiF crystal. With the thinner shims, there is a larger gap between the top surface of the crystal and the basal chord of the detector plate. This gap could allow stray, undiffracted light from the source to bounce off the far wall of the box and scatter on to the detector. It is therefore necessary to design the defining slit carefully for each shim, to ensure that the outermost rays from the source are allowed to hit only the crystal surface.

2.3.2. Dispersion.

The exact dispersion from a curved crystal can be analytically derived. The characteristics of curved crystal spectrometers are well documented[12,13,14]. The results of this

characterization are summarized here. Figure 2-7 illustrates the spectrometer geometry and notation. The SRL spectrometer differs from traditional film spectrometers in that the detector plane is flat for ease of detector placement, rather than an circular curve with origin coincident with the crystal origin. Rays of all wavelengths emitted from the source form a cone defined by aperture and stops and are incident on the bent-crystal with radius of curvature r_c. The radiation along the axis strikes the crystal at some distance δy_o below the top of the crystal and at some angle ϕ_o with respect to the vertical. The distance δy_o is the crystal shim height and is related to ϕ_o by the following equation:

$$\delta y_o = r_c(1-\cos\phi_o) \tag{2.5}$$

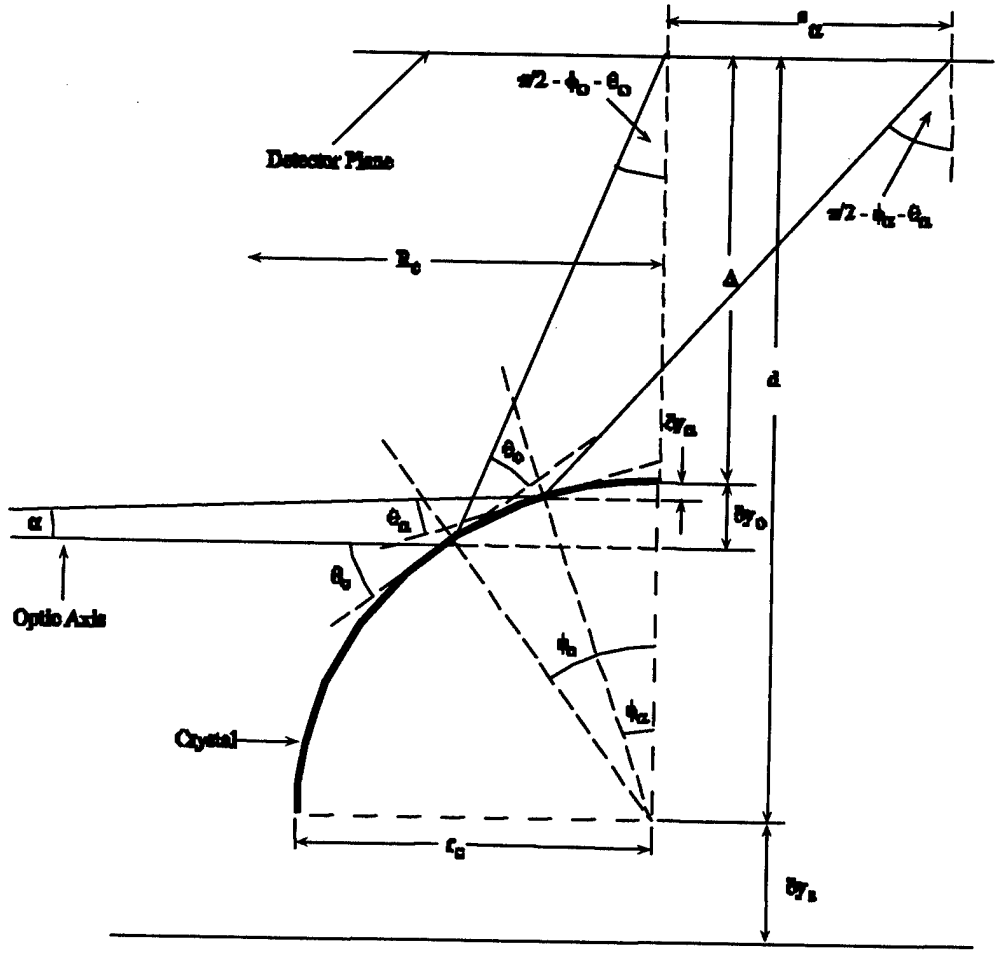

Figure 2-7. Schematic diagram showing the ray along the optic axis and one at an angle α from the optic axis

Other rays incident at angles α with respect to the axis strike the crystal surface at an angle ϕ at a distance y_α below the crystal top. Among the axial rays incident on the crystal, only those with integral number n of wavelengths λ_o satisfy the Bragg condition

$$\eta\lambda_o = \delta(\sin\theta_o + \sin\theta_x) \tag{2.6}$$

are diffracted to some horizontal location $s_\alpha=0$ on the detector plane. Here, δ is the spacing between crystal planes, and θ_o is the angle of incidence relative to the crystal plane which is just the tangent plane at the point of incidence. The angle θ_x is the exit angle and for first order $n=1$, $\theta_x = \theta_o$. For the optic axis parallel to the base of the crystal, $\theta_o = \phi_o$. For all other rays at angle α with respect to the optic axis and incident at ϕ_α, then $\theta_\alpha = \phi_\alpha - \alpha$ and only those rays with wavelength γ_α which satisfy the Bragg condition

$$\eta\lambda_\alpha = \delta(\sin(\phi_\alpha - \alpha) + \sin\theta_x) \tag{2.7}$$

are diffracted to the detector plane at some location s_α. The angle α is defined as

$$\alpha = \tan^{-1}\left(\frac{\delta y_\alpha - \delta y_o}{R_c}\right) \tag{2.8}$$

where δy_α is the distance below the crystal top that the ray at α strikes the crystal, and R_c is the source distance from the crystal origin for the axial ray.

If the distance d between the crystal origin and the detector plane is set such that the axial ray, which may correspond to the K-edge of the observed plasma, is diffracted to the center of the detector plane ($s_\alpha=0$) then:

$$\begin{aligned} d &= r_c(\cos\phi_o + \sin(\phi_o)\tan(2\phi_o)) \\ &= r_c\cos\phi_o\left(1 + \frac{2\sin^2\phi_o}{\cos 2\phi_o}\right) \end{aligned} \tag{2.9}$$

The detector plane center is defined to be that location directly above the vertical crystal edge. Equivalently, for $\Delta=d - r_c$ the distance between the top of the crystal and the detector plane,

$$\Delta = r_c\left(\cos\phi_o + \sin(\phi_o)\tan(2\phi_o) - 1\right) \tag{2.10}$$

Because $\phi_o=cos^{-1}(1-\delta y_o/r_c)$, Δ is also just a function of δy_o for a given r_c.

From the ray optics shown in Figure 2.7, the distance s_α that a ray of wavelength λ_α is diffracted from the center of the detector plane is given by:

$$s_\alpha = \frac{\Delta + r_c(1-\cos\phi_\alpha)}{\tan(2\phi_\alpha - \alpha)} - r_c\sin\phi_\alpha \tag{2.11}$$

Except near the top of the crystal, $\alpha << \phi_\alpha$ and $\theta_\alpha=sin^{-1}(\eta\lambda/\delta - sin\theta_x) \approx \phi_\alpha$ and these equations reduce to:

$$s_\alpha \approx \frac{\Delta + r_c(1-\cos\phi_\alpha)}{\tan(2\phi_\alpha)} - r_c\sin\phi_\alpha \tag{2.12}$$

$$\approx r_c\left(\frac{k-\cos(\sin^{-1}(\eta\lambda/\delta - \sin\theta_x))}{\tan(2\sin^{-1}(\eta\lambda/\delta - \sin\theta_x))} - \sin^{-1}(\eta\lambda/\delta - \sin\theta_x)\right) \tag{2.13}$$

where $k= 1+ \Delta/r_c$. Equation 2.13 is plotted in Figure 2-8 for $n=1$ and several values of k. The normalized line position s_α/r_c is a nearly linear function over a wide range of $\lambda/2\delta$, $0.2\leq\lambda/2\delta\leq 0.8$, for a given k. To avoid strongly nonlinear regions, practical spectrometer designs are limited to $s_\alpha\leq 1.5\ r_c$ for small k. From Figure 2-8, there is a design tradeoff between increased linearity for large k and a reduced wavelength range for a fixed detector plane length.

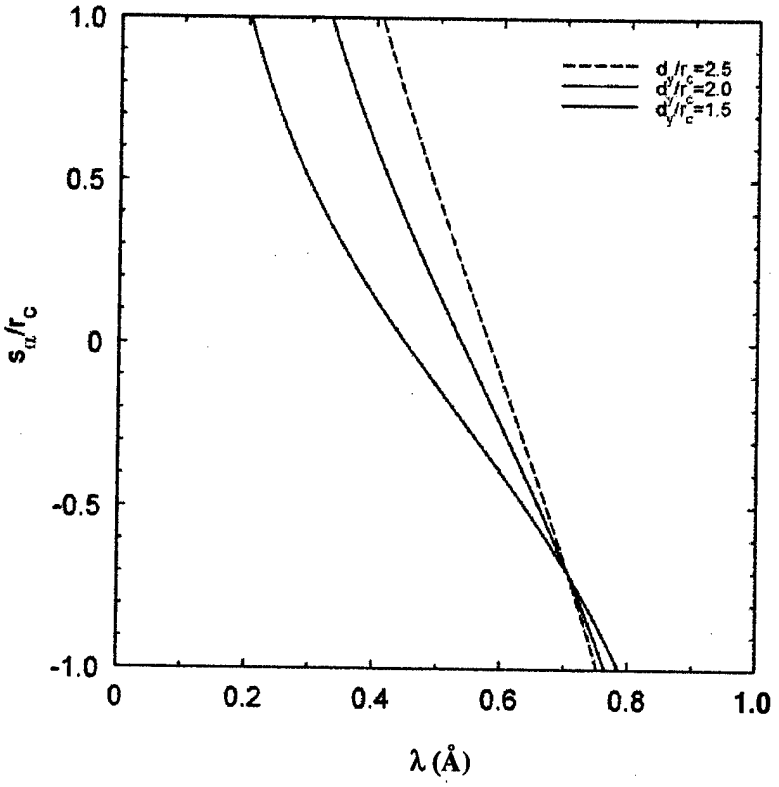

Figure 2- 8. Normalized distance along film plane s_α/r_c as a function of the normalized wavelength $\lambda/2\delta$.

The spectrometer dispersion function $d\lambda/ds$ is given by the expression,

$$\frac{d\lambda}{ds} = \frac{2\delta}{r_c}\cos\theta_\alpha\left(\frac{\sin\theta_\alpha}{\tan 2\theta_\alpha} - \frac{2(k-\cos\theta_\alpha)(1+\tan^2 2\theta_\alpha)}{\tan^2 2\theta_\alpha} - \cos\theta_\alpha\right) \qquad (2.14)$$

Figure 2-8 also contains dispersion curves corresponding to the wavelength location curves from Equation.2.13.

A computer code was written to solve for the dispersion with the KAP crystal. With this code it is possible to determine the dispersion, the height of the crystal tangent above the beam line center (the crystal shim height) and the distance between the crystal and the center of the detector plane, for a given X-ray source to crystal distance. Figure 2-9 shows the dispersion and the location along the detector plane for a KAP crystal with shim

height of 7.6 mm, a crystal to detector distance of 96.6 mm, and a source to crystal distance of 1000 mm. The entire neon spectrum in this case is dispersed on to one half of the detector plane. The 15 cm long detector plane captures X-rays extending from 6 Å to 18 . Å The dispersion is a function of wavelength and ranges from 0.03 Å /mm to 0.14 Å /mm. This allows for the largest dispersion. A slit, located at the entrance of the spectrometer, can be designed to limit any stray radiation, yet allow the crystal to be properly illuminated. For using the spectrometer on the SRL Dense Plasma Focus (DPF) source, the slit must be 10.3 mm in the direction perpendicular to the width of the crystal.

The crystal spectrometer was designed to be easily adapted for use on sources other than the SRL source. The crystal dispersion code can be used to design the crystal shim and detector heights for any given spectrum and crystal material. For example, if the aluminum spectrum from an aluminum Z-pinch on PHOENIX were to be studied, a MICA crystal could be used and the spectrometer located 3 m from the source. Figure 2-10 shows the dispersion of a MICA crystal, designed for the aluminum spectrum. The crystal shim height would be 4.3 mm and the crystal to detector distance would be 68.9 mm. The 15 cm wide detector plane captures X-rays extending from 2 Å to 17 Å. The dispersion ranges from 0.03 Å /mm to 0.18 Å /mm.

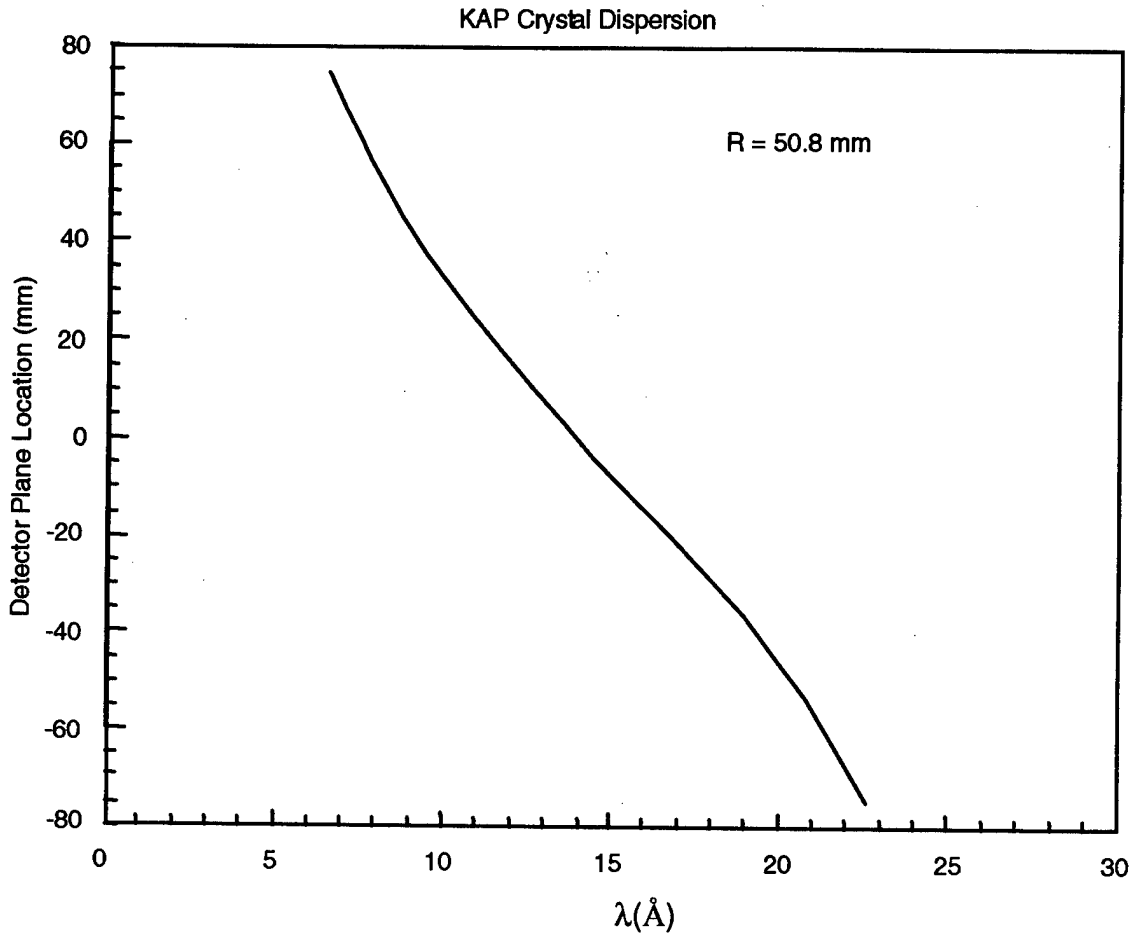

Figure 2- 9. Dispersion from a KAP crystal with a shim height of 7.6 mm.

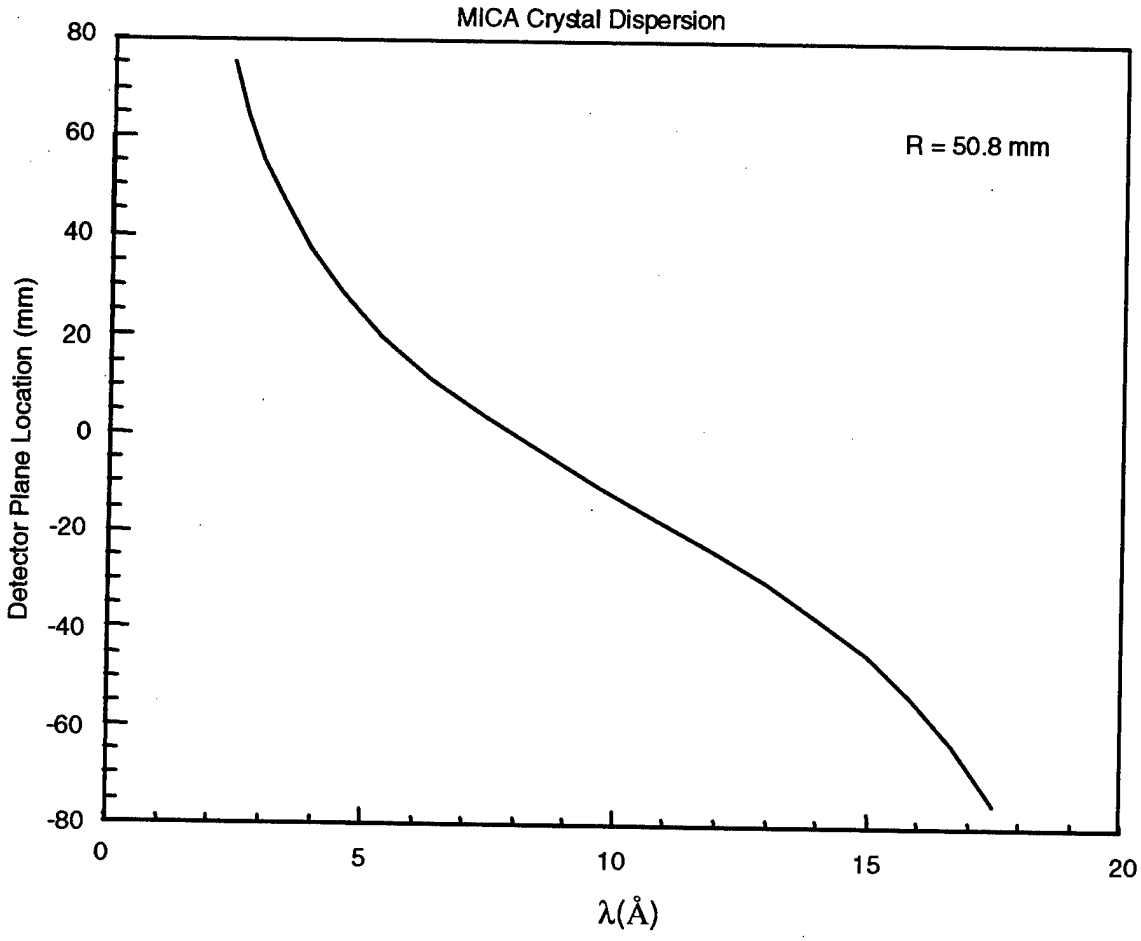

Figure 2-10. Dispersion from a MICA crystal with a shim height of 4.3 mm.

2.3.3. The X-ray crystal spectrometer.

Figure 2-11 shows a photograph of the X-ray crystal spectrometer. The spectrometer is compact and rugged. The three main components of the spectrometer are the base, the lid and the housing. Figure 2-11 also shows the crystal mounted on the base of the spectrometer. The crystal can pivot about an axis parallel to the beam-line. It can also be translated in a direction perpendicular to the beam-line axis. Spectra of different elements can be captured using shims of different heights and adjusting the detector plate to crystal distance. The lid of the spectrometer showing the detector plate with the several of the 24 PIN diodes mounted on it is also shown in Figure 2-11. The detector plate has grooves milled in it that allow DEF film to be used to capture the spectrum. The PIN diodes can then be located at the spectral bands of interest using the millimeter rule attached to the detector plate.

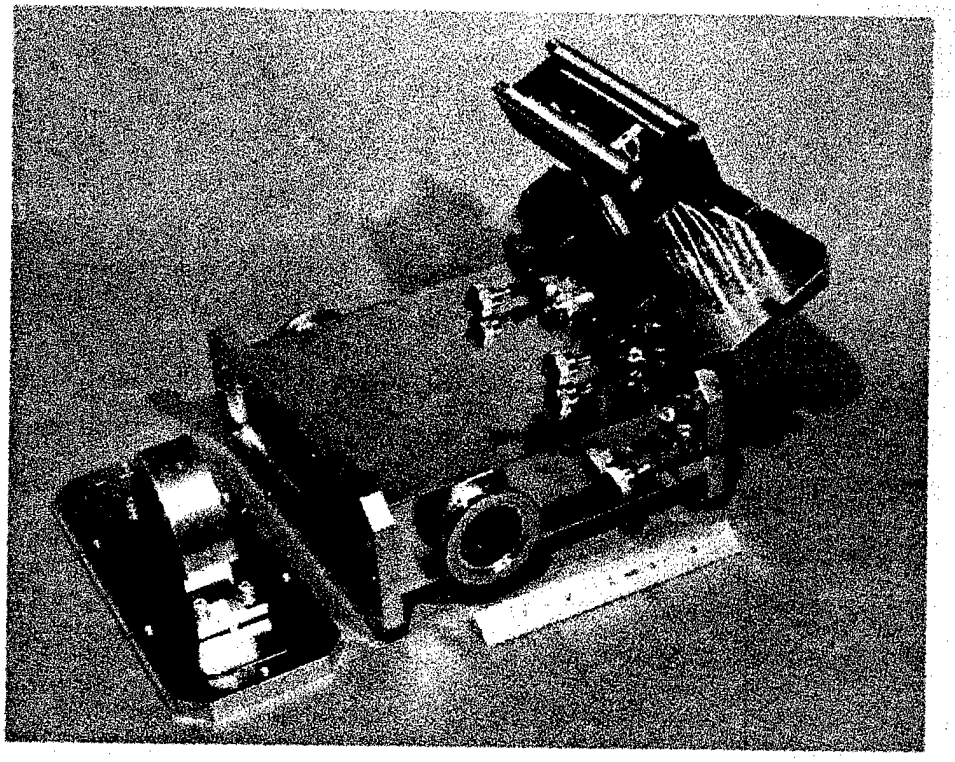

Figure 2-11. Photograph of the bent-crystal spectrometer.

Table 2-3. Expected spectrometer signal strength on DECADE.

	Al	Ar	Cu	Kr
K-shell energy (keV)	1.5-2.5	3.2-4.5	8.4-10.0	13.2-15.0
K-shell output (kj)	600	360	10	6
Source distance (m)	3	3	2	2
Signal strength (V)	12-120	7-70	0.5-4.5	0.3-2.5

2.3.4. Addition of spatial resolution.

Spatial resolution is easily added to the time resolved X-ray crystal spectrometer developed in this effort by making two simple design changes:

- The first change is to replace the 8 individual PIN diodes by 8 linear arrays of 3 PIN diodes each. The diameter of each diode in the array is 2 mm.
- The second change is to add a cross-slit in the beam-line that is ~ 100 μ m x ~ 20 mm and located with its long dimension perpendicular to the width of the crystal. The slit spatially resolves the emissions along the width of the crystal. In order to achieve 0.5 mm spatial resolution at the source, the slit must be located such that it provides a 4:1 magnification at the detector plane. This is achieved on DECADE, with the spectrometer located at 3000 mm from the source, by placing the cross-slit 600 mm from the source.

If the source to spectrometer distance were reduced to 2000 mm, the same resolution could be achieved by locating the cross-slit at 400 mm from the source. Since this location is rather close to the source, it would be preferable to locate the cross-slit at 667 mm from the source and achieve a 2:1 magnification at the detector plane. With the 2 mm diameter PIN diodes used in the crystal

spectrometer built under Phase I SBIR effort, the resolution at the source would be 1 mm. However, these can be replaced by diodes that are 1 mm in diameter, again producing a resolution of 0.5 mm at the source.

In order to study aluminum spectra, the KAP crystal would be replaced by the MICA crystal described in Section 2.3.2. As shown in Figure 2-11 this crystal (with a 50.8 mm radius of curvature), when mounted on a shim of height 4.3 mm with a detector to crystal distance of 68.9 mm provides adequate dispersion to resolve the K-shell spectrum from aluminum. The height of the slit (in the direction perpendicular to the crystal width) at the entrance of the spectrometer required to eliminate spurious illumination within the spectrometer is 7.6 mm. The shorter dimension of the slit, designed to provide spatial resolution, would be the same as that discussed in the preceding paragraphs.

2.4 DATA ACQUISITION SYSTEM.

To obtain time resolved data from spectrometers or pinhole cameras the community has been using MCPs. The images produced on the MCPs are captured on film and later digitized. This approach does not provide quantitative information, since the film is a highly non-linear detector and its response varies dramatically with the development process used for the particular piece of film. One way around the problem is to use charge coupled device (CCD) detector arrays to image the output of the MCPs. While this does away with the inherent errors of using film, it comes with its own set of problems. CCD detectors are rather sensitive to the harsh EMP environment that exists near PRS simulators such as PHOENIX, SATURN, *etc* and care must be taken to shield the instruments. In addition, the MCPs still have be gated synchronously with the X-ray pulse, a problem which is made rather difficult by the fact that the pinch tie often varies from shot to shot.

The silicon PIN diodes utilized by SRL eliminates the need for film detectors or even CCD detector arrays. However, the large number of pixels in the PIN diode array demands a large number of digitizer channels. At speeds of 500 MS/s (required to capture the essentials of a ~ 30 ns X-ray pulse) present digitizer technology is expensive and bulky.

SRL approached ASA Instruments, with the problem of multiple channel array digitization at high speeds in a compact module. ASA developed for SRL a 224-channel digitization system capable of digitizing at 500 MS/s and storing a 1 μ s long record, based on a new analog sampling array (500 channels at 200 MS/s with an analog bandwidth of 125 MHz) presently under development. The signal-to-noise ratio is better than 60 dB with channel to channel cross-talk limited to 40 dB. The system was based on a standard VXI bus crate. Each digitizer board contains 32 channels, requiring a total of 7 digitizer boards. Only one timing module was required to provide the timing signal to all 7 digitizer boards, making the use of timing fiducials unnecessary. A total of 9 timing channels are available on the timing module providing for future addition of digitizer boards. Including the standard VXI controller, the entire 224 channel system used only 9 of the available 13 slots on the single VXI bus, leaving 4 slots for future expansion. This system provides a low cost multi-channel digitization capability that does not exist at the present time. The record length of 1 μs allows the digitizers to capture the PIN diode output over the entire duration of the current pulse in simulators such as DECADE and thus avoids the problem of the need for coincidence of the time gates on MCPs with the X-ray pulses. The overall digitizer package in the standard VXI crate fits in a 48.3 cm (19″) rack mount housing which is <60 cm (<24 ″) tall.

The digitizers communicate with an external data analysis micro-computer using the GPIB interface. ASA provided command and control procedures based on the LabWindows software. SRL has written software based on the industry standard graphics program IDL (Interactive Data Language), for image display and analysis. This package was selected in conjunction with PHOENIX personnel based on experience both facilities shared with this software package. The image display program provides animation of the X-ray and XUV pinhole camera images and displays the spectrum as a function of space and time. Image analysis programs were written to obtain quantitative information from the images, such as minimum pinch radius, the velocity of implosion, the total output energy in selected wavelength bands, and the output power in selected wavelength bands.

SECTION 3
EXPERIMENTAL RESULTS

3.1 SRL TESTING.

After design and fabrication of the bent-crystal spectrometer and the X-ray and XUV camera bodies, all three instruments were assembled and leak tested to $\approx 1 \times 10^{-7}$ Torr. The spectrometer was the first of the three instruments to be tested using X-rays. The spectrometer design was identical to the instrument previously delivered to PHOENIX under DSWA contract #DNA001-92-C-0102 with the exception of the spatial resolution capability added to the present instrument. Extensive verification of the instrument design was performed using the SRL/DPF and reported at length in the Final Report[15]. For initial tests, the 3 X 8 diode array was installed. Because the 224 channel digitizer was not available at the time, the spectrometer was mounted on a X-ray monochromator illuminated by a Manson source[16] located in the Astronomy Department at Boston University. While these DC sources have low beam current ($\leq$ 1 mA) and low X-ray flux, the energy range ($\leq$ 10 kV) was appropriate for spectrometer operation. PIN diode currents, typically ≈ 0.1 μ A, were monitored with an electrometer. Operation of the spectrometer and the diodes was verified using a magnesium oxide anode (E_{Mg}=1.3 keV).

After receipt of the digitizer, X-ray camera verification was possible. For this test, the 10 X 10 array of unfiltered diodes was installed in the camera. The diodes were biased to 20 V using the circuit shown in Figure 3-1. A total of 224 channels were built using state-of-the-art printed circuit board techniques and components. Channels were arranged 10 to a board and the boards were installed into two standard width, 48 cm (19 in), chassis. The onboard diode bias power supply can provide up to 50 V back bias to the PIN diodes. The DC bias is blocked from each digitizer channel, represented by its input resistance R_{in} = 50Ω, by a blocking capacitor C.

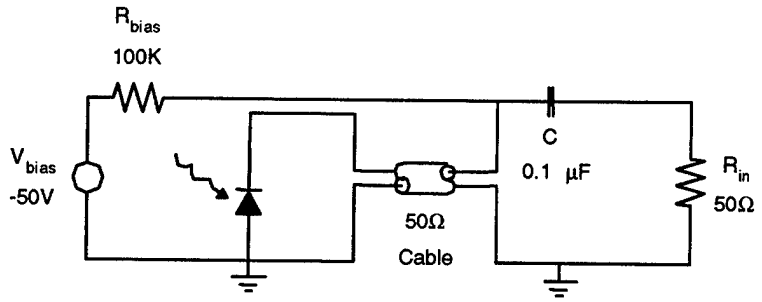

Figure 3-1. PIN diode bias circuit.

The SRL/DPF X-ray source was used to test the X-ray camera. This X-ray source is an 0.3 MA Z-pinch and produces ~ 10 - 15 J pulse of neon K-shell emissions with a pulse duration ~ 10 - 15 ns and can be operated at repetition rates of up to 2 pps. Electrical energy stored in a 57.6 μ F capacitor bank is switched into the X-ray source by 6 triggered rail-gap switches. As the quartz insulator between the two electrodes in vacuum breaks down a current sheath is formed on its surface. This sheath is propagated along the length on the cylindrical, coaxial electrodes by the JXB force, and sweeps cold neon ahead of it. As it reaches the end of the electrodes the JXB force develops a radial component due to the billowing of the current sheath. This radial force induces a radial collapse of the neon plasma, heating it and increasing its density to form a hot dense pinch along the axis of the electrodes (see Figure 3-2). X-rays are emitted by this pinch for about 10 - 15 ns. The actual device is shown in Figure 3-3.

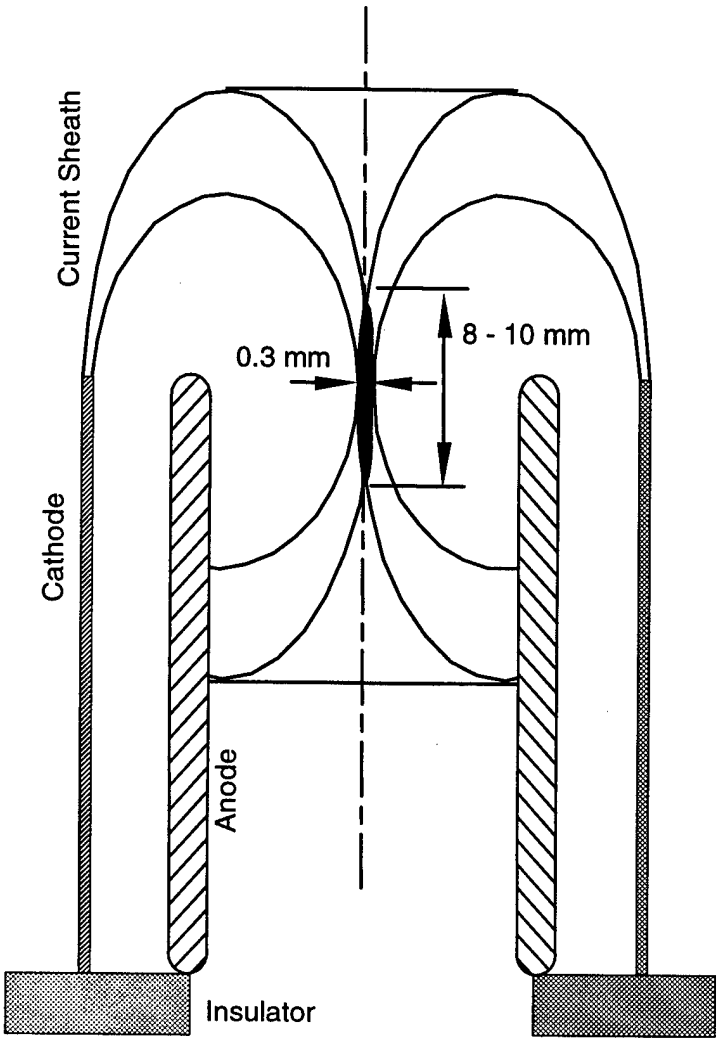

Figure 3-2. Schematic diagram showing the DPF dynamics and radial collapse.

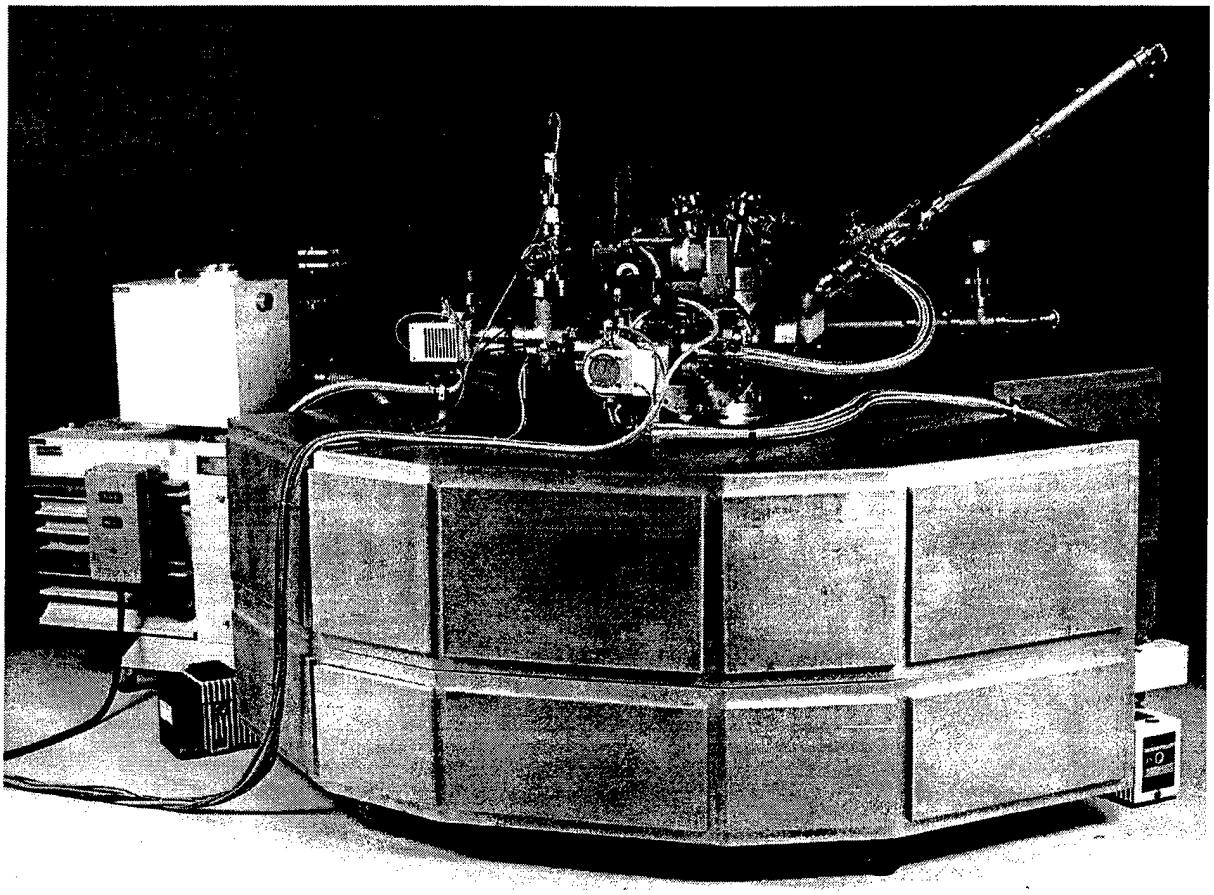

Figure 3-3. SRL Z-pinch.

The camera was mounted below the pinch providing an end-view of the discharge. This location was selected because it minimized the possibility of debris damage and maximized the viewing chord length and therefore the X-ray flux. The distance from the pinch to the detectors was 80 cm. Initial tests were conducted with no pinhole to determine the baseline noise level and whether any light paths existed that would contribute to a baseline signal level. These tests established that the noise level was ≈ 2 mV. Next a very wide aperture (5 mm X 5 mm) was inserted to provide uniform illumination of the diode array and provide a relative calibration of each of the diodes. Figure 3-4 shows a 10 X 10 X-ray camera image of a typical 2 Torr neon plasma and Figure 3-4 shows the temporal behavior of the diode signals. The diode array was positioned near the X-ray image edge to show the noise floor in addition to the average signal level.

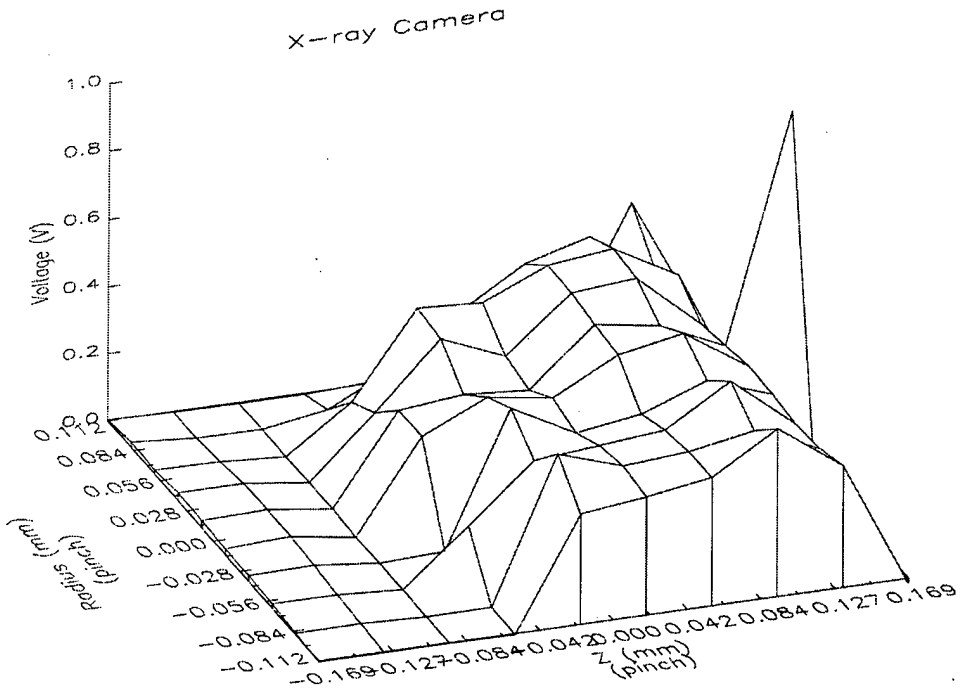

Figure 3-4. Spatial X-ray camera diode signals for neon on the SRL/DPF.

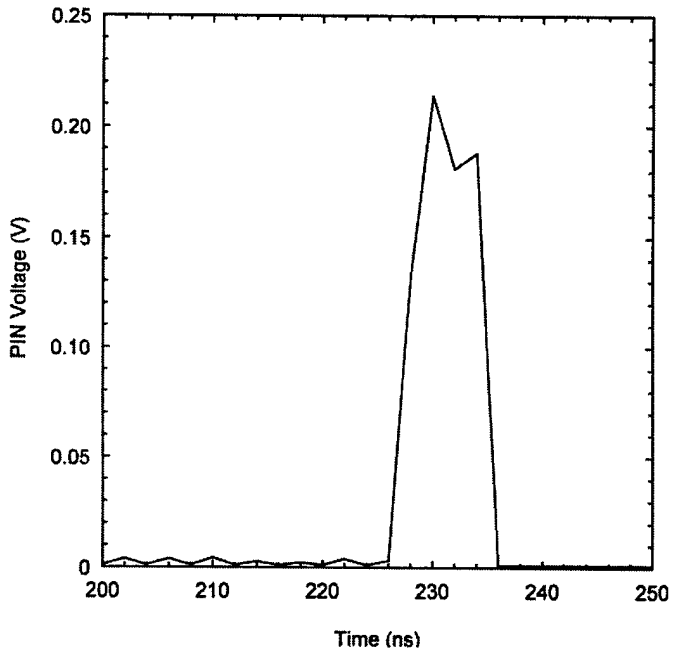

Figure 3-4 (continued). Spatial X-ray camera diode signals for neon on the SRL/DPF.

The image in Figure 3-4 was produced by data analysis software written by SRL around the standard data analysis and plotting program package IDL.

Soon after the X-ray camera was tested at SRL, the spectrometer, the X-ray camera, and the digitizer were delivered to PHOENIX for installation and validation.

3.2 PHOENIX TESTING.

The bent-crystal spectrometer and the X-ray camera were delivered to the Naval Surface Warfare Center/PHOENIX on June 3, 1996 with one week of experimental time available for validation. Upon arrival, the SRL X-ray imaging digitizer and diode-bias circuitry were installed in the User Room, partially filling the single rack provided by the PHOENIX facility. A partial compliment of cables (124) were already installed by the PHOENIX staff and were readily connected to the PIN diode bias circuits and the X-ray diagnostics.

Normally, ≈ 15 shots are possible in one week, however, during this particular week, only 5 shots were available because of vacuum problems associated with a gas nozzle system. The spectrometer was installed along with a 200 μ m X 5 mm slit. The slit and the spectrometer initially were oriented parallel to the Z-pinch axis to provide spatial resolution in the radial direction. Electron temperature and X-ray energy variations are strongest in the radial as opposed to the axial direction and this measurement would maximize information on the run-in of the plasma. DEF film spectra were obtained after some alignment of the slit/spectrometer system. Diodes were positioned in locations determined by the film image however they were not ready before the end of the week of experimental time.

Initial alignment of the X-ray pinhole camera was with a 50 μm pinhole provided no image. Larger pinholes were installed to facilitate alignment. After several realignments and the eventual removal of the pinhole, a signal was seen on the X-ray camera. Under these conditions, the diodes are uniformly illuminated. Figure 3-5 shows the diode array signals for shot PH1195 which was a Ar/Kr discharge. The temporal history of one of the PIN diodes is shown in Figure 3-6. At this point, the week of PHOENIX experimental time was complete, and the PHOENIX device was made ready for the users following SRL.

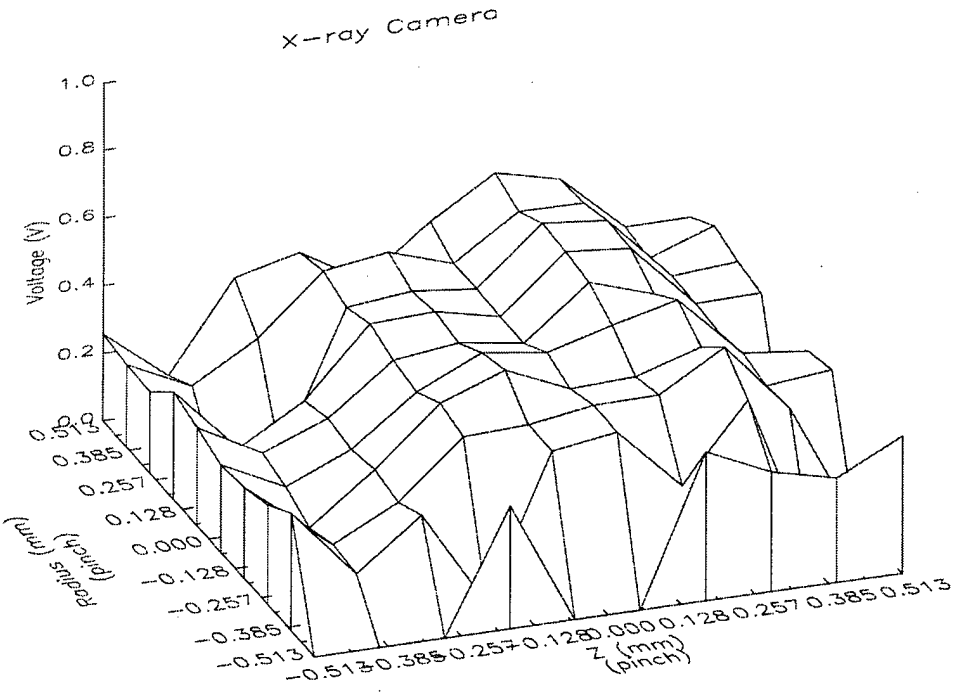

Figure 3-5. Spatial X-ray camera diode signals for Ar/Kr on PHOENIX.

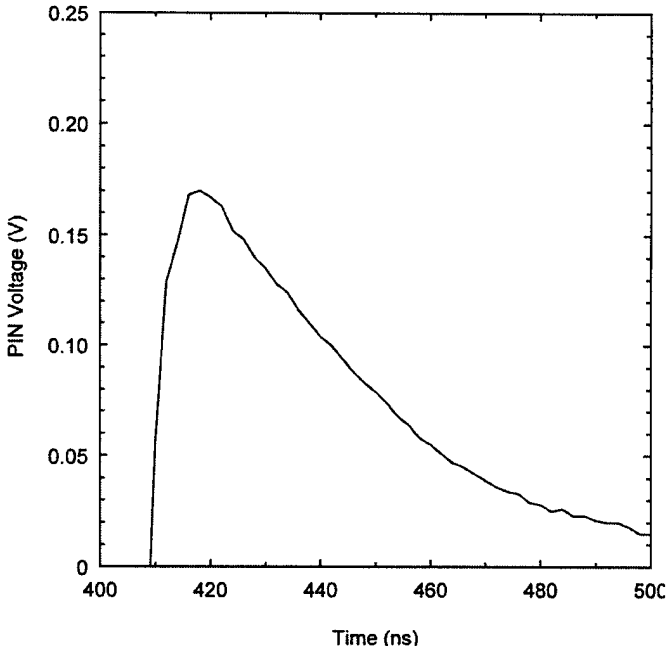

Figure 3-6. Temporal X-ray camera diode signals for Ar/Kr on PHOENIX.

During the validation week, a User Manual was provided to the PHOENIX staff, and instruction was conducted on the use of the digitizer and data analysis software.

During the following weeks, PHOENIX staff members used the spectrometer and the X-ray camera/digitizer systems. Spectrometer alignment remained problematic so the orientation was rotated to provided axial spatial resolution. Additional film and PIN diode data was taken. The X-ray pinhole camera system was also used however periodic reports from PHOENIX personnel to SRL indicated that the diode signal level was decreasing.

After receipt of the grazing incidence mirror, the XUV camera was assembled and a second trip the NSWC was scheduled for the week of July 22, 1996. Upon arrival at PHOENIX, SRL personnel installed the XUV camera on the diagnostic port previously occupied by the X-ray camera. In this process, they determined that the degradation of the X-ray camera signals was a result of contamination of the PIN diode surfaces by a light-brown haze. It is well known that diode sensitivity to X-rays is a strong function of surface conditions, and the temporal accumulation of this unknown material reasonably accounts for the reported decrease in diode signal strength. The identity of this material may be related to a vacuum leak in or near the X-ray camera.

The XUV camera was in the process of alignment when a catastrophic failure of PHOENIX occurred after only 3 shots. The remainder of the week was dedicated to repair work of PHOENIX. As a result of the X-ray camera alignment difficulties, DEF film was incorporated into the XUV camera alignment process. Preliminary alignment consisted of inserting a film pack, in place of the camera body, after the grazing incidence mirror. These images indicated X-rays were indeed reflected from the nickel mirror and were striking the film in the anticipated location.

Also during this visit, SRL personnel installed upgraded digitizer control and data analysis software. The software changes reflected the concerns and issues expressed by PHOENIX personnel from the first installation visit. The GPIB interface between the digitizer crate and the remote user data analysis computer was implemented. Revised User Manuals were provided to document the additional features. Training was also

provided to additional PHOENIX personnel on the use of the digitizer and data analysis software.

SRL has maintained contact with PHOENIX personnel after the end of the present Phase II contract to ensure continued successful operation of the X-ray diagnostic suite. In these communications, it has been learned that the diodes in the XUV camera now also show an accumulation of the same material that coated the X-ray camera diodes. At the shutdown of PHOENIX the diodes will be shipped to their manufacturer, IRD, Corp. for analysis and cleaning.

SECTION 4

REFERENCES

1. R. Spielman, *et al.* Sandia Labs. Report SANDxxx, UC-xxx (inpreparation).

2. D. Mosher, S.J. Stephanakis, K. Hain, C.M. Dozier, and F.C. Young, Ann. New York Acad. Sci. **251**, 632 (1975).

3. T. Nash, C. Deeney, P.D. LePell, R. Prasad, and M. Krishnan, Rev. Sci. Instrum. **61**, 2804 (1990), 2807 (1990), 2810 (1990).

4. M. Krishnan, C. Deeney, T. Nash, P.D. LaPell, and K. Childers, *Second Intern. Conf. on Dense Z-Pinches*, AIP Conf. Proc. **195,** 17 (1989).

5. C. Deeney, T. Nash, R.R. Prasad, L. Warren, K.G. Whitney, J.W. Thornhill, and M.C. Coulter, Phys. Rev. A **44**, 6762 (1991).

6. J.L. Guiliani, Jr., J.E. Rogerson, C. Deeney, T. Nash, R.R. Prasad, and M. Krishnan, J. Quant. Spectrosc. Radiat. Transfer **44**, 471 (1990).

7. K.G. Whitney, J.P. Apruzese, J.W. Thornhill, and J. Davis, "Scaling Z-pinch Plasmas with Atomic Number for a Given K-shell Emission", NRL Memo Report 6579, November 17, 1989.

8. Applied Electron Corp., Quantrad Sensor Division, Silicon PIN Diode Specification Sheet, 1991.

9. B.L. Henke, P. Lee, T.J. Tanaka, R.L. Shimabukuro, and B.K. Fujikawa, At. Data Nuc. Data Tab. **27**, 1 (1982).

10. Dr. Raj Korde, IRD, Inc., personal communication, 1991.

11. Science Research Laboratory Phase I SBIR Final Technical Report, "Instrument suite to measure space and time resolved XUV and X-rays from Z-pinches", Contract #DNA001-92-C-0102, March 23, 1993.

12. B.L. Henke, "Low Energy X-Ray Spectrometer with Crystals and Multilayers" in *AIP Conf. Proc. on Low Energy X-Ray Diagnostics*, ed. David T. Attwood and Burton L. Henke, Monterey, CA, 1981, **75**, 85 (1981).

13. P.G. Burkhalter, D.B. Brown, and M.Gersten, J. Appl. Phys. **52**, 4379 (1981)

14. D.B. Brown and M. Fatemi, J. Appl. Phys. **51**, 2540, (1980).

15. Science Research Laboratory Phase I SBIR Final Technical Report, "Instrument Suite to Measure Space and Time Resolved XUV and X-rays from Z-pinches", Contract #DNA001-92-C-0102, March 23,1993.

16. Austin Instruments, Redding, MA, designed by Dr. J.E. Manson.

DISTRIBUTION LIST

DSWA-TR-97-4

DEPARTMENT OF DEFENSE

BALLISTIC MISSSILE DEFENSE OFFICE
ATTN: T/SL

DEFENSE INFORMATION SYSTEMS AGENCY
ATTN: COMMANDER

DEFENSE INTELLIGENCE AGENCY
ATTN: DT - 4A
ATTN: DT - 4C
ATTN: TWJ

DEFENSE SPECIAL WEAPONS AGENCY
ATTN: ES, JOAN MA PIERRE
2 CY ATTN: ESA
ATTN: ESA, G DAVIS
ATTN: ESA, W SUMMA
ATTN: ESE, R C WEBB
ATTN: ESE, W J SCOTT
ATTN: EST, K WARE
ATTN: EST, L PRESSLE Y
ATTN: EST, R GULLICKSON
ATTN: EST, R SCHNEIDER
ATTN: OPS
ATTN: PMPO
ATTN: PMPO, P HEBERT
2 CY ATTN: TRC
ATTN: WEL
ATTN: WEP, T KENNEDY

DEFENSE TECHNICAL INFORMATION CENTER
2 CY ATTN: DTIC/OCP

FC DEFENSE SPECIAL WEAPONS AGENCY
ATTN: FCT - S G BALADI
ATTN: FCTI
ATTN: FCTO
ATTN: FCTR, R W SHOUP

NATIONAL DEFENSE UNIVERSITY
ATTN: NWCO

NATIONAL SECURITY AGENCY
ATTN: TECHNICAL LIBRARY

OFFICE OF THE SEC OF DEFENSE
ATTN: DOCUMENT CONTROL

DEPARTMENT OF THE ARMY

ARMY RESEARCH LABORATORIES
ATTN: TECH LIB
ATTN: AMSRL-WT-NH/ KEHS
ATTN: AMSRL-WT-KEHS

ARMY SPACE & STRATEGIC DEFENSE COMMAND
ATTN: CSSD-ES-E1, R CROWSON

DEFENSE ADVANCED RESEARCH PROJECTS AGENCY
ATTN: DED

DEP CH OF STAFF FOR OPS & PLANS
ATTN: DAMO-ODW

US ARMY WAR COLLEGE
ATTN: LIBRARY

U S ARMY VULNERABILITY ASSESSMENT LAB
ATTN: SLCVA - TAC

US ARMY THAAD PROJECT OFFICE
ATTN: CSSD-WD

DEPARTMENT OF THE NAVY

NAVAL SEA SYSTEMS COMMAND
ATTN: PMS 423

NAVAL RESEARCH LABORATORY
ATTN: CODE 6720, J DAVIS
ATTN: CODE 6770, G COOPERSTEIN

NAVAL SURFACE WARFARE CENTER
ATTN: B DEPARTMENT

OFFICE OF NAVAL INTELLIGENCE
ATTN: DEOO
ATTN: LIBRARY

NAVAL AIR SYSTEMS COMMAND
ATTN: AIR 5161
ATTN: AIR - 5164
ATTN: AIR - 933

SPACE & NAVAL WARFARE SYSTEMS CMD
ATTN: PNW - 145
ATTN: TECHNICAL LIBRARY

DEPARTMENT OF THE AIR FORCE

AFIWC/MSO
ATTN: TECHNICAL LIBRARY

AIR FORCE CTR FOR STUDIES & ANALYSIS
ATTN: AFSAA/SAI, RM 1D363 THE PENTAGON

AIR UNIVERSITY LIBRARY
ATTN: AUL - LSE

PHILLIPS LABORATORY
ATTN: PL/WSP, J KIUTTU
ATTN: WSP, J DEGNAN

SAN ANTONIO AIR LOGISTICS CTR
ATTN: ALC SW, MR F CRISTADORO

SSP - 27334 TRIDENT
ATTN: J BURTLE
ATTN: K TOBIN

USAF ROME LABORATORY TECH LIBRARY, FL2810
ATTN: RBCM
ATTN: RBCT

USAF/AEDC/DOT
ATTN: DOT, MAJ J ROWLEY

DEPARTMENT OF ENERGY

LAWRENCE LIVERMORE NATIONAL LAB
ATTN: L - 477, L SUTER
ATTN: L - 84, G SIMONSON

LOS ALAMOS NATIONAL LABORATORY
ATTN: D - 410, C EKDAHL
ATTN: MS D408
ATTN: MS F617
ATTN: MS H827
ATTN: MS - J970, R REINOVSKY

SANDIA NATIONAL LABORATORIES
ATTN: M HEDEMANN
ATTN: M K MATZEN
ATTN: D COOK
ATTN: TECH LIB
ATTN: W BALLARD
ATTN: W BEEZHOLD

U S DEPT OF ENEREGY IE - 24
ATTN: D CRANDALL

U S DEPARTMENT OF ENERGY
ATTN: C B HILLAND, DP - 243
ATTN: C KEANE, DP - 16
ATTN: OMA/ DP-252, R GUNDERSON

OTHER GOVERNMENT

CENTRAL INTELLIGENCE AGENCY
ATTN: OSWR/ SSD/SWB
ATTN: OSWR/STD/TTB
ATTN: OSWR, J PINA

FEDERAL EMERGENCY MANAGEMENT AGENCY
ATTN: SL- CD - MP

DEPARTMENT OF DEFENSE CONTRACTORS

ALME AND ASSOCIATES
ATTN: JOHN F DAVIS
ATTN: S SEILER, G101

APTEK, INC.
ATTN: T MEAGHER

BERKELEY RSCH ASSOCIATES, INC.
ATTN: N PEREIRA

CHARLES STARK DRAPER LAB, INC.
ATTN: LIBRARY

DEFENSE GROUP, INC
ATTN: ROBERT POLL

E - SYSTEMS, INC.
ATTN: TECH INFO CTR

HY- TECH RESEARCH CORP.
2 CY ATTN: E J YADLOWSKY

INSTITUTE FOR DEFENSE ANALYSES
ATTN: TECH INFO SERVICES

JAYCOR
ATTN: M TREADAWAY

JAYCOR
ATTN: CYRUS P KNOWLES

KAMAN SCIENCES CORP.
ATTN: CLAUDE FORE

KAMAN SCIENCES CORPORATION
ATTN: DASIAC
ATTN: DASIAC/DARE

KETCH CORP.
ATTN: FRANK DAVIES

LOGICON R AND D ASSOCIATES
ATTN: E QUINN
ATTN: I VITKOVITSKY

LOGICON R AND D ASSOCIATES
ATTN:ROGER LEWIS

MAXWELL TECHNOLOGIES
ATTN: JOHN THOMSON
ATTN: PHIL COLEMAN
ATTN: WILLIAM H RIX

MISSION RESEARCH CORP.
ATTN: K STRUVE

MISSION RESEARCH CORP.
ATTN: J R HENLEY

PRIMEX PHYSICS INTERNATIONAL
ATTN: B FAILOR
ATTN: C STALLINGS
ATTN: J RIORDAN
ATTN: P SINCERNY
ATTN: S L WONG

PULSE SCIENCES, INC.
ATTN: I D SMITH
ATTN: P W SPENCE
ATTN: TECHNICAL LIBRARY

SCIENCE APPLICATIONS INTL CORP
ATTN: W CHADSEY

SCIENCE RESEARCH LABORATORY, INC
2 CY ATTN: WILLIAM GUSS

SRI INTERNATIONAL
ATTN: ELECTROMAG SCI LAB TECH LIB

SVEDRUP INC AEDC
ATTN: L S CHRISTENSEN
ATTN: V KENYON

TEXAS TECH UNIVERSITY
2 CY ATTN: L HATFIELD
2 CY ATTN: M KRISTIANSEN

THE AEROSPACE CORP
ATTN: LIBRARY ACQUISITION
ATTN: T PARK